LICENTIATE THESIS

# Digital holographic interferometry in a disturbed environment

Henrik Lycksam

LULEÅ UNIVERSITY OF TECHNOLOGY

LULEÅ
UNIVERSITY
OF TECHNOLOGY

# Digital holographic interferometry in a disturbed environment

Henrik Lycksam

Luleå University of Technology
Department of Applied Physics and Mechanical Engineering
Division of Experimental Mechanics

Printed by Universitetstryckeriet, Luleå 2009

ISSN: 1402-1757
ISBN 978-91-7439-000-1

Luleå 2009

www.ltu.se

# Abstract

Digital holographic interferometry is an optical measurement technique that is capable of measuring the movement/deformation of an object surface with extremely high accuracy, spatial resolution and temporal resolution. But, because it is very sensitive to disturbances, it is mostly used in well controlled laboratory environments. An exciting new application of the method could be for process supervision in the manufacturing industry. But before it can be used in such an environment it must be made more insensitive to disturbances. The work in this thesis deals with post processing of data from holographic interferometry measurements to reduce the effects of mechanical vibrations and random refractive index fluctuations in the surrounding air. The first approach of using a purely temporal interference filter was successful in reducing the noise due to vibrations, but the noise from the air disturbance was only reduced over a very limited spatial region. A more complete spatio-temporal filter that is not of the interference type requires that the spatio-temporal statistics of the noise from the air can be measured. Therefore the rest of the work is devoted to this problem. The method developed is applied to the relatively simple case of locally homogenous/isotropic refractive index fluctuations generated in a small wind tunnel. There is a simple theory for these types of fluctuations for which the method was successfully verified.

# Table of content

# 1 Introduction

Digital holographic interferometry is an optical measurement technique that is capable of measuring the movement/deformation of an object surface with extremely high accuracy, spatial resolution and temporal resolution. Unfortunately it is very sensitive to disturbances such as mechanical vibrations among the optical components and random refractive index fluctuations in the surrounding air. The work in this thesis deals with describing these disturbances and to find a way of post-processing the measured data to remove the noise from these disturbances. To my knowledge there is not so much work done in the field of interferometry measurements of changing objects through a turbulent medium. The problem of noninterferometric imaging through turbulent medium, such as the atmosphere, has been frequently studied in the literature and therefore a short summary of this subject is presented in section 2. Section 3 describes the principles of holographic interferometry and gives a summary of the work in the appended papers listed in section 4.

# 2 Wave propagation in random medium

It has been known for a very long time that the atmosphere somehow alters the light from the distant stars causing them to twinkle. Newton noted that the performance of telescopes would eventually be limited by the air above us which is in "perpetual tremor". His solution was to place the telescope on a mountaintop to reduce the amount of disturbed air above it. During the first half of the 1900's however, optical and mechanical technology advanced to a point that not even the best observing sites in the world could provide air that was calm enough. This was the main motivation for the development of general theories for wave propagation through random media (WPRM) that started in the late 1940's. Most of the work in this subject until the beginning of 1960's was done by Soviet scientists and summarized in the very influential monographs of Chernov [1] and Tatarskii [2] published in both the Soviet Union and United States during 1960 and 1961. Wave propagation in random media is a very interdisciplinary subject with applications in atmospheric optics and acoustics, ocean acoustics, geophysics, radio physics, plasma physics, bioengineering, condensed matter physics etc. The following is meant as a short introduction to the subject of WPRM covering some of the basic topics. Focus will be on theories for light propagation in the neutral atmosphere.

Random media can be roughly divided into two main categories: turbulent media and turbid media. In the case of light propagation through the atmosphere the important parameter of the medium is the refractive index. In a turbulent media the refractive index variations are smooth and coarse compared to the wavelength of light. The variations are also very small compared to the mean refractive index. The clear neutral atmosphere is a perfect example of a turbulent medium. In a turbid media the refractive index variations are much larger and in the form of discrete particles with a size comparable to the wavelength of light. Turbid media are more difficult to deal with since absorption, wide angle scattering (including backscattering) and depolarization effects must be included. Examples of turbid media are clouds, smoke and other aerosols.

## *2.1 Stochastic processes*

Before going into some theories of wave propagation through random media it is necessary to know something about stochastic processes (random functions). An example of a stochastic process is the temperature distribution $T(\mathbf{r},t)$ in the atmosphere which varies randomly in both space and time. There are two ways of thinking about a random function such as $T(\mathbf{r},t)$. Imagine that we measure the temperature distribution during some time interval. If we could turn back time and do the measurement again the result would be different. The random process

$T(\mathbf{r},t)$ can be thought of as the collection of all such possible measurements together with the probability that they are measured. This is a very intuitive way of thinking that is often very useful. Different statistical quantities such as the expectation value of the temperature at $(\mathbf{r},t)$ can be thought of as being calculated as mean values taken over all these possible functions (ensemble averaging). A more quantitative way of describing a random process is to think of it as a collection of random variables. For each space-time point $(\mathbf{r},t)$ the random process $T(\mathbf{r},t)$ is just a random variable. To describe the process we need to specify the probability distribution for each random variable. But since we know that the temperature fluctuations in nearby space-time points are highly correlated these random variables will not be independent. In theory it would be possible to specify the joint probability density function for all these (infinitely many) variables but most often it is sufficient just to know the correlation between two arbitrary space-time points. Thus the stochastic process $T(\mathbf{r},t)$ can often be sufficiently described by two functions: its expected value $\eta(\mathbf{r},t)$ and correlation $B(\mathbf{r_1},\mathbf{r_2};t_1,t_2)$:

$$\begin{aligned} \eta(\mathbf{r},t) &= \langle T(\mathbf{r},t) \rangle \\ B(\mathbf{r_1},\mathbf{r_2};t_1,t_2) &= \langle T(\mathbf{r}_1,t_1) \cdot T(\mathbf{r}_2,t_2) \rangle \end{aligned} \tag{1}$$

where $\langle\ \rangle$ is the expectation value operator. If a fast and sensitive temperature probe is set to measure the temperature fluctuations at a point in the atmosphere for a few minutes it will be seen that the nature of the fluctuations will be the same over the whole measurement. Specifically the average temperature around which the fluctuations occur will be constant and the intensity and time scales of the fluctuations are also the same. In equation (1) this means that $\eta(\mathbf{r},t) = \eta(\mathbf{r})$ and $B(\mathbf{r_1},\mathbf{r_2};t_1,t_2) = B(\mathbf{r_1},\mathbf{r_2};\tau)$ where $\tau = t_2 - t_1$. This property of a stochastic process is called stationarity. There are few processes that are completely stationary. The type of stationary just defined is called wide sense stationarity. In the previous example if the measurement time is increased to a few hours there will be changes in both the average temperature and the intensity and timescale of the fluctuations. The atmospheric temperature is an excellent example of a process with a type of stationarity called stationary time increments. This means that the fluctuations are a combination of very rapid variations (on the order of ms to s) combined with much slower variations with periods of days, years or even thousands of years. For this type of stationarity it is much better to describe the similarity of fluctuations between two space-time points using the structure function $D(\mathbf{r_1},\mathbf{r_2};t_1,t_2)$:

$$D(\mathbf{r_1},\mathbf{r_2};t_1,t_2) = \left\langle \left[ T(\mathbf{r}_1,t_1) - T(\mathbf{r}_2,t_2) \right]^2 \right\rangle . \tag{2}$$

By subtracting the temperatures instead of multiplying them the slow changes in average temperature are cancelled out and if the fluctuation strength and timescale remains the same then $D(\mathbf{r}_1,\mathbf{r}_2;t_1,t_2)=D(\mathbf{r}_1,\mathbf{r}_2;\tau)$. At a specific time the random variation in atmospheric temperature is composed of structures of all sizes, from several thousands of kilometers to a few millimeters. As mentioned in the next section the large structures are highly unpredictable whereas the smaller ones always behave in the same way. By taking the difference between the temperatures in equation (2) the effect of the large-scale variations (larger than the separation $|\mathbf{r}_2-\mathbf{r}_1|$) are effectively cancelled out and therefore the structure function always have the same functional form, depending only on $\rho=|\mathbf{r}_2-\mathbf{r}_1|$:

$$D(\rho;\tau)=\left\langle\left[T(\mathbf{r}_1,t_1)-T(\mathbf{r}_2,t_2)\right]^2\right\rangle. \tag{3}$$

A random process $T(\mathbf{r},t)$ that has this property is called a locally homogenous and isotropic process. The word locally is added because the correlation function in equation (1), that depends on structures of all sizes, does not have this behavior. Note that even though the functional form of $D(\rho;\tau)$ is the same there can still be large local variation in the strength of the fluctuations.

## 2.2 Refractive index model of the atmosphere

The most common model for the refractive index distribution in the atmosphere starts with a decomposition in the form:

$$n(\mathbf{r},t,\lambda)=n_0(\mathbf{r},\lambda)+n_1(\mathbf{r},t). \tag{4}$$

Here $n_0$ is the deterministic part of $n$ describing for example the dependence of $n$ with height over ground (due to the decrease in air density with height) and the slow daily variations due to different amount of sunlight. These variations are often so slow that they can be ignored. The effect of the turbulent fluctuations is described by $n_1$. Since $n_1$ is only a small fraction of the mean refractive index $n_0$ the dispersion due to these small fluctuations can often be ignored. The refractive index of air is a function of both temperature and pressure. Since air has very poor thermal conductivity, random temperature variation have a very long life-time compared to pressure differences that are equalized by pressure waves traveling at the speed of sound. Therefore all random refractive index fluctuations can be attributed to temperature variations. These variations are formed at a very large scale due to nonuniform heating of the earth by the sun and then successively broken down by turbulent winds to

smaller and smaller sizes that moves along with the air flow. To further simplify things it is customary to assume that the random refractive index variations do not change or evolve during the time it takes them to drift across the field of view of a telescope with the local wind speed. This means that it is possible to exclude the time dependence of $n_1$, concentrating only on its spatial properties. An excellent description of this assumption (known as Taylor's hypothesis) and its limitations can be found in [3].

All turbulent flows contain spatial structures with a huge variation in size. In 1922 Richardson proposed the energy cascade hypothesis [4] which says that in a turbulent flow (to which there is a steady input of energy) the largest structures are successively broken down to smaller ones and thus turbulent energy is transferred to smaller and smaller spatial scales until, at some critical size, energy is dissipated due to the viscosity of the fluid. In a series of papers starting in 1941 Kolmogorov made three additional hypotheses which quantified the energy cascade to something that could be used in calculations. The original articles are mostly in Russian but an excellent review can be found in [5]. For our purposes there are two important results that need to be remembered. When the structures have been broken down beyond a certain size (called the outer scale size) they start to become statistically homogenous and isotropic and thus completely independent of the macroscopic flow geometry. Also the relative distribution of turbulent energy among the different scale sizes starts to follow a certain functional form independent of the flow geometry. The range of scale sizes between the outer scale just defined and the inner scale where the structures start to disappear due to viscous dissipation is called the inertial subrange. In most manmade turbulent flows through pipes and channels of different kinds the inertial subrange is of very limited importance because it covers a very small range of scale sizes and most of the turbulent energy is found in larger structures. In the atmosphere the situation is different. The inertial subrange typically ranges from a few millimeters up to about 100 meters and even though there is a lot of turbulent energy in scale sizes larger than the outer scale these structures will be so large that they cause virtually no variation at all across the field of view of even the largest of telescopes. The distribution of turbulent energy among the different scale sizes of the refractive index fluctuations is described by the power spectral density of $n_1$ and from Kolmogorovs work we know that in the inertial subrange it has the form:

$$\phi(\kappa) = 0.033 C_n^2 \cdot \kappa^{-11/3} \tag{5}$$

where $\kappa$ is the wavenumber which is proportional to the reciprocal of the eddy size. The parameter $C_n^2$ is called the structure constant and is a measure of the

strength of the refractive index fluctuations. Note that, because the fluctuations are isotropic, $\phi(\kappa)$ is a function of only the magnitude of the wavenumber.

## 2.3 Phase and amplitude fluctuations

The earliest theoretical work on light (and sound) propagation through the turbulent atmosphere was mostly centered on the geometrical optics approximations. Figure 1 shows the geometry of the propagation problem. An initially plane wave enters a medium with random refractive index fluctuations described by $n(x,y,z,t)$. It propagates a distance $L$ through it until its amplitude $A(x,y,z,t)$ and phase $\phi(x,y,z,t)$ distributions are finally detected in the xy-plane. The meaning of the word phase needs some clarification. At a fixed point $(x_1,y_1)$ in space the magnitude of the electric and magnetic field vectors oscillate extremely rapidly in time ($\sim 10^{14}$ Hz). The phase of this oscillation is much too fast to be able to resolve with an ordinary camera. At $(x_2,y_2)$ the field vectors oscillate with the same frequency. But since the optical path length from the source to the detector is slightly different at this point, due to the random refractive index fluctuations, the oscillations will slightly out of phase and it is this "phase difference" ($\phi(x,y,z,t)$) that is the important quantity.

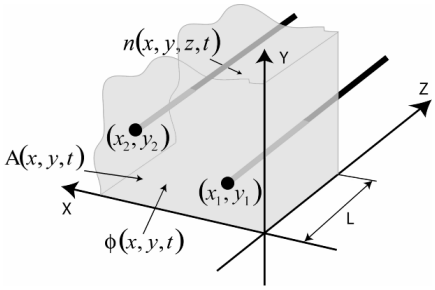


**Fig 1:** *Geometry of the propagation problem*

Using the expression (5) for the power spectral density of the refractive index fluctuations together with the equations of geometrical optics it is possible to derive the structure function of the phase fluctuations and the correlation function of the amplitude fluctuations (see section 2.1). The fact that the amplitude fluctuations have a wide sense stationary correlation function will be explained in connection with figure 2. The amplitude correlation function cannot be expressed in closed form and therefore only the mean square amplitude fluctuation (which is often sufficient information) is given:

$$D_\phi(\rho) = 2.91 \cdot k^2 \cdot L \cdot C_n^2 \cdot \rho^{5/3}, \quad l_0 << \rho << L_0$$
$$\left\langle \left( \log \frac{A}{A_0} \right)^2 \right\rangle = 2.46 \cdot C_n^2 \cdot L^3 \cdot l_0^{-7/3} \quad . \tag{6}$$

Here $\rho$ is the distance between the points $(x_1, y_1)$ and $(x_2, y_2)$ in figure 1. $L$ is the distance of propagation trough the medium, $l_0$ and $L_0$ are the inner and outer scales of the turbulence, $A_0$ is the amplitude of the undisturbed light and $C_n^2$ is a measure of the strength of the refractive index fluctuations. Because the equations of geometrical optics doesn't include the bending of light due to diffraction the equations (6) are only valid for short propagation distances (on the order of tens of meters [6]) and therefore attention was soon turned to wave optics solutions to the propagation problem. The equation that is to be solved is the stochastic wave equation:

$$\nabla^2 E(\mathbf{r}, t) + k_0^2 \varepsilon(\mathbf{r}, t) E(\mathbf{r}, t) = 0 \tag{7}$$

where $k_0$ is the vacuum wavenumber of the monochromatic wave and $\varepsilon(\mathbf{r}, t)$ the random dielectric constant of the medium. It is possible to write (7) as a scalar equation in $E$ because the depolarization term which couples the components of $E$ can be ignored as long as the wavelength is much smaller than the size of the smallest inhomogenities [7]. Unfortunately it is not known how to solve (7) exactly because $\varepsilon(\mathbf{r}, t)$ is a coefficient of $E(\mathbf{r}, t)$. The most well known way of approximately solving (7) is by perturbation theory, the simplest of which is the Born approximation [8]. In this solution it is assumed that the light wave is diffracted by only a single turbulent structure on its way from the source to the observer. (It is also assumed that the size of the refractive index fluctuations is small so that the diffraction angles are small). As the length of the propagation path increases the effects of multiple diffractions (or scatterings) start to become important. Bourret [9] was the first to include multiple scattering effects to the problem of wave propagation in random medium using the diagram technique of Feynman described in [6]. Tatarskii and Klyatskin [3] came up with a different approach, referred to as the Markov approximation. In Bourret's work the approximations and averaging procedures are done at the end after a set of exact equations have been derived. In the Markov approximation the averaging takes place at the outset and then a series of approximate equations are found for the various statistical moments. It is interesting to note that the expression for the phase structure function is the same in all of the theories mentioned above (both geometrical and wave optics solutions), a fact that will be made clear in a moment.

The first quantitative experiment to verify the theories was carried out in 1958 by Gurvich et al. [6] who measured the log amplitude fluctuations in a light beam propagating a rather short distance in a weakly fluctuating medium. They noticed good agreement with both the geometrical optics and early wave optics (Born approximation) solutions. In 1965 Gracheva et al. [10] were the first to notice a phenomenon known as saturation in the log amplitude fluctuations. As they increased the propagation length beyond that used in Gurvich's experiment they noticed that the amplitude fluctuations didn't increase indefinitely as suggested by the theory but soon approached a constant value. The length before this happens depends on the strength of the fluctuations. In 1974 Clifford et al. [11] came up with a physical explanation of the saturation phenomenon.

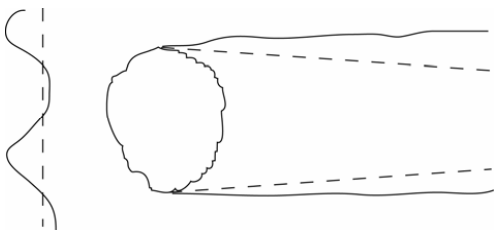

**Fig 2:** *Physical model of the saturation process.*

As illustrated in figure 2 the atmosphere is assumed to be filled with irregular eddies of different size, shape (because the medium is statistically isotropic they must be roughly spherical) and refractive index. These eddies act as random lenses which focuses or defocuses the light incident on them. This is the origin of the amplitude fluctuations. Using only the lens formula and some simple geometry it is possible to derive the same results as in equation (6) (except for the numerical constants) and also to include the effects of diffraction [6]. Because the smaller eddies have shorter focal lengths (still on the order of several kilometers) they cause larger amplitude changes and therefore are responsible for most of the amplitude fluctuations. The smaller eddies are all within the inertial subrange and are thus locally homogeneous and isotropic and therefore the amplitude fluctuations have a wide sense stationary correlation function as mentioned earlier. Figure 2 shows two light waves incident on a typical eddy (or random lens). The plane wave (dashed line) is focused by the eddy and hence at some distance to the right of it there will be a strong increase in the amplitude of the light. If, however, the light has already been focused and defocused by a large number of other eddies the wavefront might look like the solid line. In this case the light entering the lens will not be fully coherent and the eddy will not be able to focus the light as effectively as before. This is the basic physical explanation of the saturation effect. The reason that the phase fluctuations don't saturate is that they are caused by changes in the velocity along the propagation path of a light ray and it doesn't matter if the light is

coherent or not across the eddy. Diffraction effects are not important either because the fact that a light ray is not perfectly straight but follows a somewhat random path through the atmosphere doesn't significantly effect the phase fluctuations [6]. This is the reason why all of the theories mentioned above result in the same expression for the phase structure function.

## *2.4 Improvement techniques*

When observing a distant light source such as a star it is only possible to measure the intensity (square of the amplitude) distribution. To measure the phase distribution it is necessary to use special techniques such as holography described in section 3.1. There are three broad classes of methods to improve the quality of intensity images captured through the turbulent atmosphere: adaptive optics, pure post-processing techniques and methods that combine adaptive optics with post-processing. An excellent review of the basic principles of adaptive optics systems and combination techniques such as image deconvolution can be found in [12]. The basic principle of post-processing techniques is that an image captured with an exposure time that is shorter than the fluctuation time of the turbulence contains much higher spatial frequency information about the object than a corresponding long exposure image. This fact was first observed by Labeyrie [13] in 1970. The short exposure images will have a grainy speckle-like appearance due to random variations in light amplitude over the image and post-processing techniques are therefore often referred to as speckle imaging techniques. These amplitude variations are due to the propagation through the atmosphere (as described in connection with figure 2) and low-light detection noise. The routine for extracting high spatial frequency information is as follows. First a series of short exposure images of the object is taken. The number of images necessary depends mostly on the brightness of the object (a brighter object means less low-light detection noise). Typically the exposure time needed to freeze the atmospheric fluctuations ranges from a few tens of a millisecond to a few milliseconds [12]. The next step is to Fourier transform the intensity distribution in each image to produce a series of intensity spectra $I(f_x, f_y)$ where $f_x$ and $f_y$ are the spatial frequencies in the x- and y-directions in the images respectively. The intensity spectra can be expressed in terms of its modulus $|I(f_x, f_y)|$ and phase $\phi(f_x, f_y)$ as:

$$I(f_x, f_y) = |I(f_x, f_y)| \cdot \exp[i \cdot \phi(f_x, f_y)]. \tag{8}$$

The next step is to calculate the modulus squared of each image and then average this over the entire series of images to produce an estimate of $\langle |I(f_x, f_y)|^2 \rangle$ where $\langle\ \rangle$ is the expectation value operator. Let's define the

spectrum of the object irradiance distribution as $O(f_x, f_y)$ and the combined optical transfer function of both the telescope and atmosphere as $H(f_x, f_y)$. The measured average modulus squared of the intensity spectra can now be written as:

$$\left\langle \left| I(f_x, f_y) \right|^2 \right\rangle = \left| O(f_x, f_y) \right|^2 \cdot \left\langle \left| H(f_x, f_y) \right|^2 \right\rangle . \tag{9}$$

There are no brackets around $O(f_x, f_y)$ because it is assumed to be constant during the time of the measurement. Assume for the moment that instead of a series of short exposures a single long exposure with intensity spectra $I_L(f_x, f_y)$ was captured. Just as before $I_L$ can be written in terms of $O$ and $H$ as:

$$I_L(f_x, f_y) = O(f_x, f_y) \cdot \left\langle H(f_x, f_y) \right\rangle . \tag{10}$$

Although it is a bit involved, it can be shown (se for example [12]) that $\left\langle \left| H(f_x, f_y) \right|^2 \right\rangle$ is a much wider function than $H(f_x, f_y)$ and hence $\left\langle \left| I(f_x, f_y) \right|^2 \right\rangle$ contains information of higher spatial frequencies of the object than $I_L(f_x, f_y)$. In order to estimate the combined optical transfer function $H(f_x, f_y)$ a series of images of a nearby reference star is also captured (preferably just before or just after the images of the object). Since the star is more or less a point source its irradiance spectra will be constant and the average squared modulus $I_R(f_x, f_y)$ of these reference images will be:

$$\left\langle \left| I_R(f_x, f_y) \right|^2 \right\rangle = C \cdot \left\langle \left| H(f_x, f_y) \right|^2 \right\rangle \tag{11}$$

where $C$ is a constant depending on the brightness of the star. The absorption of the atmosphere is rather small at optical wavelengths and hence $\left\langle \left| H(0,0) \right|^2 \right\rangle \approx 1$ and it is possible to normalize equation (11) to get an estimate of $\left\langle \left| H(f_x, f_y) \right|^2 \right\rangle$. This is then used in equation (9) to estimate the modulus of the object irradiance distribution. Note that the quality of this estimation will be worse for higher spatial frequencies where $\left\langle \left| H(f_x, f_y) \right|^2 \right\rangle$ is small. This is because of the low-light detection noise in the detector and the estimation errors due to the finite number of images and the fact that the object and reference images aren't measured at the same time. Therefore, instead of just dividing equations (9) and (11) it is

customary to use a wiener filter to reduce the noise at high spatial frequencies [12].

The above procedure only gives the modulus of the object irradiance $\left|O\left(f_x, f_y\right)\right|$. Before an actual image can be obtained from an inverse Fourier transform the relative distribution of phases for the spectral components are also needed. Two of the most common techniques for estimating the object phase distribution are the cross-spectrum [14], [15] and bispectrum [16]. A detailed review of both methods can be found in [12]. The basic principle of both methods are the same. By estimating various statistical moments of the measured intensity spectra it is possible to get high-spatial-frequency information about the object phase spectrum. Unfortunately the result of applying these methods is a linear combination of the phase at different spatial frequencies rather than the spectrum itself. To get the phase spectra it is necessary to perform a second processing step that is similar to a phase unwrapping procedure. Therefore the retrieval of the phase is considerably more involved than the modulus. Fortunately in some important cases, such as the study of binary star separation, phase information is not needed.

# 3 Holographic interferometry

## *3.1 Basic principles*

Holographic interferometry is an optical measurement technique introduced by Powell and Stetson [17] in 1965. It enables surface deformations to be measured with an accuracy of tens of nm and spatial resolution of a few μm. With the invention of high-speed digital cameras it is now also possible to follow these deformations in time with a sampling rate of several kHz. The basic principle of the method is to capture and store holograms of the object surface taken at different times. Holograms differ from ordinary photographs in that they can capture not only the irradiance distribution of the object but also the phase distribution (see section 2.3) in the light. Because of the extremely high frequencies of optical waves the phase distribution in the light from the object cannot be measured directly. It is necessary to compare the object wave with another wave (called reference wave) by allowing them to interfere on the detector. From the interference pattern on the detector it is possible to deduce the phase distribution in the object light.
By calculating the phase difference at each point between two of the holographic images it is possible to determine how the object surface has changed. This is illustrated in figure 3.

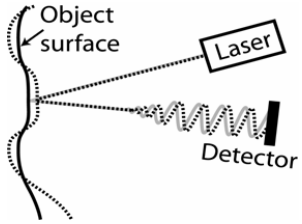


**Fig 3:** *Basic principle of holographic interferometry*

As the object surface moves the path length of the light from the laser to the detector changes. By looking at the phase difference in the detector plane it is possible to deduce how much the surface has deformed since the wavelength of the light is known. It is important to note that it is not possible to determine the absolute phase (the total number of oscillation from the laser to the detector) in a single hologram. Therefore it is important that the deformation of the object surface at all points between two successive images is less than a quarter of a wavelength. Otherwise there will be ambiguities in the determination of the phase difference.

The problem with holographic interferometry is that it requires that the only thing changing in a series of images is the object surface. In reality there will always be slight disturbances. One kind of disturbance are vibrations among the components in the measurement setup. These vibrations tend to produce measurement noise with a very high degree of spatial correlation that is concentrated in narrow frequency bands and this noise is thus fairly easy to suppress [18]. Even in the absence of mechanical vibrations it is possible to have phase changes on the detector that are not due to the motion of the object surface. This is because it is the optical path length (product of geometrical path length and refractive index) that determines the number of oscillations between the laser and detector. If the medium in which the measurement takes place has random refractive index fluctuations there will be random changes in the phase at the detector that are incorrectly interpreted as object surface deformations.
Even in a controlled laboratory environment the noise due to the surrounding air can be large enough to cause problems if the object deformation is small and if the measurement time is longer than the fluctuation time of the medium. The purpose of this work has been to develop a digital filter capable of reducing measurement noise due to random refractive index fluctuations in the air surrounding the measurement setup.

## *3.2 Filtering of measured data*

Figure 4 shows a schematic sketch of the measurement setup used in the experiments.

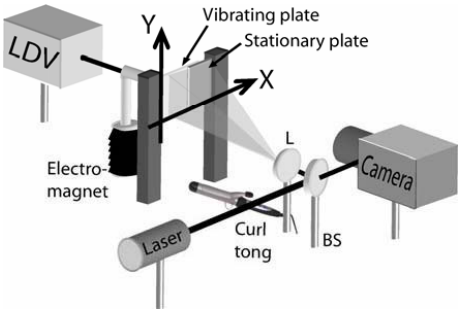


**Fig 4:** *Sketch of the measurement setup*

A thin steel plate is rigidly attached along one side while the other side is periodically bent back and forth using an electromagnet in connection with a signal generator. A small stationary plate is also inserted into the field of view of the camera as the digital filter originally used requires this. The motion of the plate at one selected point is accurately measured from the back with a laser Doppler vibrometer. In front of the plate a region of refractive index fluctuations is created using a couple of curl tongs.

The result of the measurement is a stack of images describing the distribution of phase in the light from the object at different times. Such a stack, illustrated in figure 5, is often referred to as a phase volume.

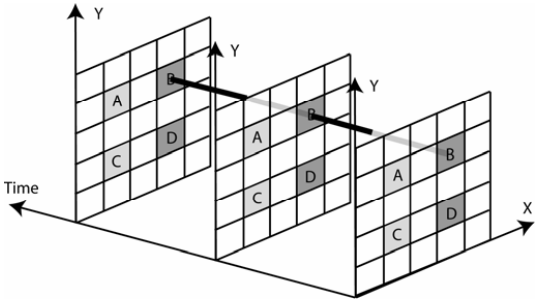


**Fig 5:** *Stack of images showing the measured phase distribution at different times.*

The measured phase will contain both the information of the object deformation/movement and the random "noise" from the refractive index fluctuations of the air in front of the object. The solid line drawn is just a time sequence describing the phase changes with time at point B. The simplest approach to filtering a phase volume such as that in figure 5 is to filter each such time sequence separately, independent from each other. This is what is done in paper A. The filtering procedure is described in figure 6.

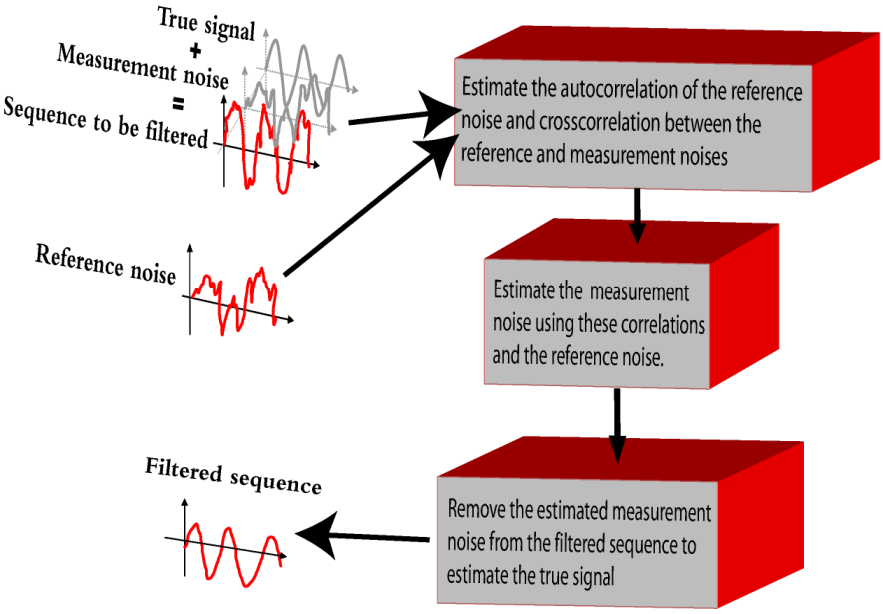


**Fig 6:** *Procedure for filtering the time sequences.*

Let's assume that the point B in figure 5 lies on the moving plate described in figure 4. Then the time sequence of phases through this point will contain the sum of a "true signal" due to the object motion and a "measurement noise" due to the refractive index fluctuations in the air. At another point A that lies on the stationary plate in figure 4 the measured phase sequence contains only the noise from the refractive index fluctuations. If points A and B lie relatively close to each other then the "measurement noise" at point B and the noise at A will be fairly well correlated. Thus if we know the noise at A and the cross correlation between the noises at A and B it should be possible to estimate the "measurement noise" at B. Then we can simply subtract this estimated noise from the phase sequence at B to get an estimate of the true signal. This is the basic principle of the filter. Since the noise measured at point A on the stationary plate is used to filter all of the other points it is referred to as the "reference noise" in figure 6. The object motion is statistically independent from the noise due to the refractive index fluctuations. Therefore the cross correlation between the noises at A and B can be calculated simply as the cross correlation between the whole phase sequences at B and A. The filter also needs the autocorrelation of the phase noise (assumed to be the same at all points) which is easily calculated at point A on the reference plate.

The obvious advantage with this type of filter is that the full spatiotemporal correlation of the phase fluctuations is not needed, only the crosscorrelations between discrete points. Also, because of the stationary plate, these correlations are easily estimated. The most serious drawback is that as the reference point A is far from the point B to be filtered the cross correlation between the noises will be small. Thus it will be difficult for the filter to correctly guess the appearance of the "measurement" noise" at B from the "reference noise" at A. Another problem is that all sequences are filtered independently and optimized to produce the best mean squared estimate over time. But there is nothing that says that the spatial distribution of the estimated phase noise at a specific time should be close to the true phase distribution.

These drawbacks suggest that it is necessary to use a full spatio-temporal filter in which the whole phase volume is filtered simultaneously. But such a filter would require that spatio-temporal statistics (e.g. correlation function) of the phase fluctuations is known. Paper B describes a method of measuring the spatio-temporal covariance (correlation) function of the phase fluctuations in a medium with refractive index fluctuations. It also suggests a way of separating the covariance function of the object deformation/motion from that of the phase fluctuations.

### *3.3 Measuring spatio-temporal phase statistics*

In this experiment we used a wind tunnel to generate the refractive index fluctuations. The reason is that the phase fluctuations produced follow a relatively simple theory which can be used to validate the method. Figure 7 shows a sketch of the home-built wind tunnel.

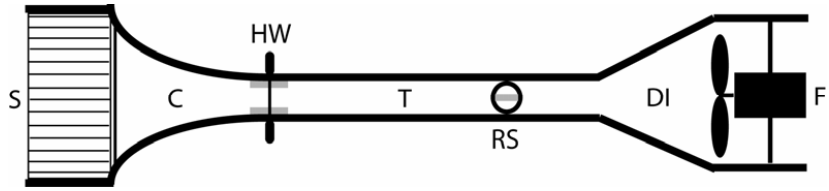


**Fig 7:** *Sketch of the wind tunnel.*

It consists of a settling chamber (S) in which the large eddies in the surrounding air are broken down. The contraction chamber (C) increases the speed of the air by reducing the cross section of the channel. At the start of the test section (T) are a couple of heated Chantal wires that produce an initial large scale temperature variation that is successively broken down to smaller and smaller structures by the turbulent motion of the air inside the channel. At the end of the test section are a pair of rotatable slits (RS) that allows light to be sent through the channel. After the test section is a diffuser (DI) where the speed of the air is decreased. At the end of the channel is the fan (F) that sucks air through the channel from left to right. The principle of the method is simple. A thin sheet of light is created and sent through the slits in the channel. The phase fluctuations across the sheet are measured with high sampling rate so that the fluctuations are resolved in time. From the measured phase fluctuations it is easy to estimate the various statistics. There are two problems to be overcome in the measurement process. First of all it is necessary for the light to pass through a diffuser plate to decode the phase. But this introduces a random phase variation that need to be eliminated. Two different ways of accomplishing this is discussed in paper B. The second problem is that the measured phase is periodic. Once it exceeds $\pi$ it wraps down to $-\pi$. Before the measured phase can be interpreted as something useful it needs to be unwrapped. In three dimensions this is very a complicated and time-consuming operation especially for large phase volumes. The phase volumes need to be large because of the need to resolve fluctuations in time combined with need to include many independent fluctuations. Paper B suggests a method of using simple temporal unwrapping instead that works for a certain class of turbulent flows.

# 4 Summary of appended papers

Paper A: Wiener filtering of interferometry measurements through turbulent air using an exponential forgetting factor.

Authors: Henrik Lycksam, Per Gren and Mikael Sjödahl.

Summary: The purpose of the paper was to develop a digital filter to improve the quality of holographic interferometry measurements performed in a disturbed environment. The filter was successful in reducing the noise due to vibrations but the noise from the air was only reduced over a small spatial region. Also because the filter is purely temporal there is no way of assuring spatial continuity in the filtered data.

Conclusions: To overcome the shortcomings of the simple temporal filter it is necessary in the future to use a full spatio-temporal filter.

Paper B: Measurement of spatio-temporal phase statistics in turbulent air flow using high speed digital holographic interferometry.

Authors: Henrik Lycksam, Per Gren, JamesLeblanc and Mikael Sjödahl.

Summary: The purpose of the paper was to develop a method of measuring the spatiotemporal phase statistics for light propagation in a medium with refractive index fluctuations. The method is verified against locally homogenous/isotropic refractive index fluctuations generated in a small wind tunnel. A way of separating the statistics of the object motion/deformation from that of the air is also suggested.

Conclusions: The measured statistics showed good agreement with theory which is taken as a validation of the method.

# 5 References


1. L. A. Chernov, *Wave Propagation in a Random Medium* (McGraw-Hill, New York, 1960).
2. V. I. Tatarskii, *Wave Propagation in a Turbulent Medium* (Dover Publications, Inc. , New York, 1961).
3. V. I. Tatarskii, *The effects of the turbulent atmosphere on wave propagation* (Israel Program for Scientific Translations, Jerusalem, 1971).
4. L. F. Richardson, *Weather Prediction by Numerical Process* (Cambridge University Press, Cambridge, 1922).
5. S. B. Pope, *Turbulent Flows* (Cambridge University Press, 2006).
6. J. W. Strohbehn, ed., *Laser beam propagation in the atmosphere* (Berlin, 1978).
7. J. W. Strohbehn, "Line-of-sight wave propagation through the turbulent atmosphere," Proceedings of the IEEE **56**(1968).
8. M. Born and E. Wolf, *Principles of optics,* 7 ed. (Cambridge University Press, Cambridge, 2005).
9. R. C. Bourret, "Stochastically Perturbed Fields, with Application to Wave Propagation in Random Media," Il Nuovo cimento **26**, 1-31 (1962).
10. M. E. Gracheva and A. S. Gurvich, "Strong fluctuations in the intensity of light propagated through the atmosphere close to the earth," Radiophys. Quant. Electron **8**(1965).
11. S. F. Clifford, G. R. Ochs, and R. S. Lawrence, "Saturation of Optical Scintillation by Strong Turbulence," J. Opt. Soc. Am. **64**(1974).
12. M. C. Roggemann, B. M. Welsh, and R. Q. Fugate, "Improving the resolution of ground-based telescopes," Reviews of Modern Physics **69**(1997).
13. A. Labeyrie, "Attainment of Diffraction Limited Resolution in Large Telescopes by Fourier Analyzing Speckle Patterns in Star Images," Astron. & Astrophys. **85**(1970).
14. K. T. Knox and B. J. Thompson, "Recovery of images from astronomically degraded short exposure images," Astrophys. J. **193**(1974).
15. K. T. Knox, "Image retrieval from astronomical speckle patterns," Journal of the Optical Society of America **66**(1976).
16. A. W. Lohmann, G. Weigelt, and B. Wirnitzer, "Speckle masking in astronomy: triple correlation theory and appplications," Applied Optics **22**(1983).
17. R. L. Powell and K. A. Stetson, "Interferometric analysis by wavefront reconstruction," Journal of the Optical Society of America **55**(1965).
18. H. Lycksam, M. Sjödahl, P. Gren, and J. Leblanc, "Wiener filtering of interferometry measurements through turbulent air using and exponential forgetting factor," Applied Optics **47**(2008).

# Paper A

Wiener filtering of interferometry measurements through turbulent air using an exponential forgetting factor

# Wiener filtering of interferometry measurements through turbulent air using an exponential forgetting factor

Henrik Lycksam,[1,*] Mikael Sjödahl,[1] Per Gren,[1] and James Leblanc[2]

[1]Division of Experimental Mechanics, Luleå University of Technology, 971 87 Luleå, Sweden

[2]Division of Signal Processing, Luleå University of Technology, 971 87 Luleå, Sweden

*Corresponding author: henrik.lycksam@ltu.se

Received 6 February 2008; accepted 14 April 2008;
posted 29 April 2008 (Doc. ID 92532); published 21 May 2008

The problem of imaging through turbulent media has been studied frequently in connection with astronomical imaging and airborne radars. Therefore most image restoration methods encountered in the literature assume a stationary object, e.g., a star or a piece of land. In this paper the problem of interferometric measurements of slowly moving or deforming objects in the presence of air disturbances and vibrations is discussed. Measurement noise is reduced by postprocessing the data with a digital noise suppression filter that uses a reference noise signal measured on a small stationary plate inserted in the field of view. The method has proven successful in reducing noise in the vicinity of the reference point where the size of the usable area depends on the degree of spatial correlation in the noise, which in turn depends on the spatial scales present in the air turbulence. Vibrations among the optical components in the setup tend to produce noise that is highly correlated across the field of view and is thus efficiently reduced by the filter. 

*OCIS codes:* 090.2880, 010.7060, 110.0115.

## 1. Introduction

Optical measurement techniques are frequently used today in all sorts of industrial applications such as manufacturing, process monitoring, and product testing. The advantages of interferometric imaging techniques are high precision and that whole deformation fields (not just single points) are acquired simultaneously. However, interferometric techniques are seldom used because of their sensitivity to both mechanical vibrations and air disturbances. Much work has been done on imaging through turbulent media (mostly the Earth's atmosphere). In 1970 Labeyrie [1] invented a technique that gives the diffraction-limited intensity autocorrelation of astronomical objects. The technique was later modified by Gough [2] to produce intensity images instead of just autocorrelations. Atmospheric turbulence is also a major problem in airborne synthetic aperture radar imaging of the earth. Here it is necessary to measure both the amplitude and the phase of the incoming light. Just as with coherent imaging with a real physical lens-system, the light at a point in a synthetic radar image can be thought to be a sum of the contributions from all point-pairs of different separation on the imaginary antenna created as the airplane or satellite moves in its orbit. Tateiba [3] has shown that atmospheric turbulence lowers the contribution to the total field for point-pairs of large separation compared with the nonturbulent case and proposes a spatial filtering method that raises the amplitude for point-pairs with high separation. More recently methods have been developed that are capable of dealing with moving objects [4], but the motion needs to be of a simple form, e.g., constant. All methods just described have one thing in common; they require the object to be stationary (or at least to have motion of an easy form) on

0003-6935/08/162971-08$15.00/0

the timescale of the atmospheric turbulence, which means that they cannot be directly applied to the case of interferometric measurement on moving or deforming objects. The purpose of this paper is to develop a method capable of reducing measurement noise caused by vibrations and air turbulence in interferometric measurements of a nonstationary object as shown in Fig. 1. With the help of a spatial carrier wave, the complex amplitude $U(x,y,t)$ of the object light is reconstructed by the Fourier filtering method [5]. The surface displacement between any two times can then be found simply by comparing the difference in (unwrapped) phase. However, the turbulent air in front of the object creates random phase shifts due to differences in optical path caused by random refractive index variations. To reduce the effects of the random phase variations, the measured data is post processed with a digital noise interference filter. The filter measures a reference noise signal on a small stationary plate that is inserted in the field of view just in front of the object and uses this to reduce noise at other points in the image.

## 2. Theory

### A. Describing the Air Turbulence

Some simplifying assumptions regarding the air turbulence will be adopted in this paper. First of all it will be assumed that there are no particles (e.g., smoke or dust) present, which means that absorption and wide angle scattering are negligible. It will also be assumed that the imaging optics are deep within the near-field of the most abundant turbulent eddies [6], which is the same as saying that scattering can be neglected so that an incoming light ray is simply phase-delayed by the medium. The validity of this assumption may be easily verified in practice by performing subimage speckle correlation of intensity images taken at different times. Now the turbulence may be characterized by a real valued function, $n(x,y,z,t)$, that is the refractive index of the air. This function will, of course, be a random function of both space and time. As shown in Fig. 2, the light from an object point $P_1$ is assumed to be divided into small solid angles in which the phase deviation for all light rays caused by the turbulent air during the propagation to the aperture of the imaging system is the same. The total complex amplitude $U_{\text{tot}}(t)$ at $P_1^*$ in the image plane can now be written as the sum of the contributions from all these solid angles:

$$U_{\text{tot}}(t) \triangleq A_{\text{tot}}(t) \cdot e^{i\cdot\phi_{\text{tot}}(t)} = \sum_j A_j \cdot e^{i\cdot\phi_j(t)}. \tag{1}$$

The phases $\phi_j(t)$ at the entrance pupil (ENP) of the imaging system for each solid angle are given by

$$\phi_j(t) = k \cdot \int_{\text{path } j} n(x,y,z,t)ds, \tag{2}$$

and the amplitudes $A_j$ will only depend on the optical properties of the object surface and the numerical aperture of the imaging system. Integration is performed along the centerline of each solid angle. Since the object surface is rough, there will also be a random phase constant at each point due to the microstructure of object. But this term will vanish when comparing the phases at different times and is therefore left out of Eq. (1). Our goal is to determine the statistical mean and autocorrelation for the total phase $\phi_{\text{tot}}(t)$ at $P_1^*$, which can be thought of as a function of $n(x,y,z,t)$ using the unwrapping operator $UW\{\}$,

$$\phi_{\text{tot}}(t) = UW\left\{\tan^{-1}\left[\frac{\text{Im}(U_{\text{tot}}(t))}{\text{Re}(U_{\text{tot}}(t))}\right]\right\} \triangleq g[\phi_1(t), \phi_2(t), \ldots, \phi_N(t)]. \tag{3}$$

It will, however, be easier to think of the function in terms of $\phi_j(t)$, because then the mapping is memoryless (the value of $\phi_{\text{tot}}(t)$ at time $t$ depends only on the value of $\phi_j(t)$ at time $t$) and will be easier to handle mathematically. From [5] we know that the statistical mean and autocorrelation of $\phi_{\text{tot}}(t)$ can be written in terms of the first- and second-order joint probability density function (PDF) for the phases $\phi_j(t)$ as

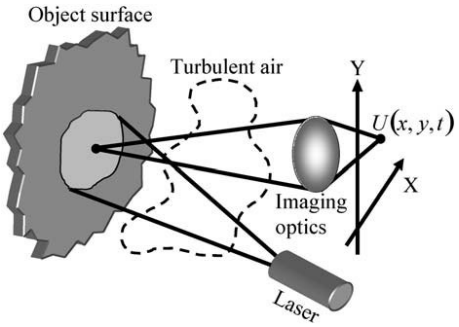


Fig. 1. Schematic of the problem. An interferometric setup measures the complex amplitude of the light from the object in an image plane as a function of time. The measurement is disturbed by a region of turbulent air between the object and imaging optics.

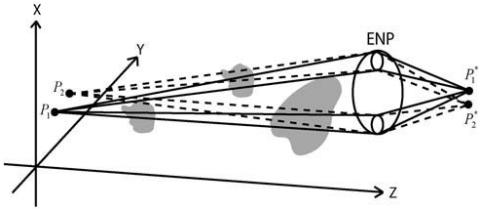


Fig. 2. Connection between the phase changes at an image point and the refractive index distribution of the turbulent air.

$$E\{\phi_{\text{tot}}(t)\} = \int_{-\infty}^{\infty}\cdots\int_{-\infty}^{\infty} g(\phi_1,\ldots,\phi_N) \cdot f_{\phi}(\phi_1,\ldots,\phi_N;t)\,d\phi_1\cdots d\phi_N, \tag{4a}$$

$$E\{\phi_{\text{tot}}(t_1)\cdot\phi_{\text{tot}}(t_2)\} = \int_{-\infty}^{\infty}\cdots\int_{-\infty}^{\infty} g(\phi_1^1,\ldots,\phi_N^1) \cdot g(\phi_1^2,\ldots,\phi_N^2)\cdot f_{\phi}(\phi_1^1,\ldots,\phi_N^1, \times\phi_1^2,\ldots,\phi_N^2;t_1,t_2)\,d\phi_1^1\cdots d\phi_N^1 \cdot d\phi_1^2\cdots d\phi_N^2. \tag{4b}$$

Hence if the first- and second-order joint PDFs for $\phi_j(t)$ are slowly varying with time, the statistical mean and autocorrelation of $\phi_{\text{tot}}(t)$ at $P_1^1$ will also have a slow time variation. It is possible, in principle, to determine the first- and second-order joint PDFs for $\phi_j(t)$ from Eq. (2), but this requires a complete characterization (PDFs of all orders) of $n(x,y,z,t)$, which is really only a theoretical artifact. But from Eq. (2) it is easy to calculate two first-order and one second-order joint moments for $\phi_j(t)$ in terms of corresponding moments of $n(x,y,z,t)$, which can be interpreted physically:

$$\begin{aligned} E\{\phi_j(t)\} &= k\cdot\int_{\text{path}\,j} E\{n(x,y,z,t)\}ds, \\ E\{\phi_m(t_1)\cdot\phi_j(t_2)\} &= k^2\cdot\int_{\text{path}\,m}\int_{\text{path}\,j} E\{n(x_1,y_1,z_1,t_1) \cdot n(x_2,y_2,z_2,t_2)\}\,ds_1 ds_2\,(m\neq j), \\ E\{\phi_j(t_1)\cdot\phi_j(t_2)\} &= k^2\cdot\int_{\text{path}\,j}\int_{\text{path}\,j} E\{n(x_1,y_1,z_1,t_1) \cdot n(x_2,y_2,z_2,t_2)\}ds_1 ds_2. \end{aligned} \tag{5}$$

The first moment of Eq. (5) describes how the expected values of the phases in the various solid angles at the ENP shown in Fig. 2 vary with time, which is shown to depend only on the expected values of the refractive index along the path of the light. If the turbulent air around the measurement system is in roughly thermal equilibrium, i.e., there is no large scale stratification of air with different temperature, then it is reasonable to assume that the expectation value of $n(x,y,z,t)$ at each point is a slowly varying function of time that changes with the net heating or cooling of the air. This means that $E\{\phi_j(t)\}$ will also be a slowly changing function of time. It will be argued later that the meaning of "slow" is "slow compared with the most important frequencies in the object movement/deformation." The second moment of Eq. (5) describes two things. For the time difference $t_2 - t_1$ that maximizes $E\{\phi_m(t_1)\cdot\phi_j(t_2)\}$, it is a measure of how correlated the phase fluctuations are over the ENP of the imaging system, which depends on the spatial scales present in the turbulence (and, of course, also the distance from the most important turbulent eddies to the ENP). On the other hand, the time difference itself is interesting because it hints whether there are global drifts of turbulent eddies in some direction across the field of view. The spatial scales and global drifts in the air turbulence will depend on the geometry and temperature distribution of the objects causing the air disturbance. It is often reasonable to assume that they are changing slowly with time, which means that for a fix time difference, $t_2 - t_1$, and two fix points, the value of $E\{n(x_1, y_1, z_1, t_1)\cdot n(x_2, y_2, z_2, t_2)\}$ will be a slow function of absolute time (note that the change with time can be due to both a changing spatial scale and a change in the global air drift, which alters the time difference for maximum correlation). This means that $E\{\phi_m(t_1)\cdot\phi_j(t_2)\}$ for a fix time difference will also be a slowly changing function of time. Finally the third moment in Eq. (5) describes the autocorrelation of the phase fluctuation in the different solid angles. Using arguments similar to those above, it is clear that for $t_2 - t_1$, the value of the autocorrelation changes slowly with absolute time. The fact that the first- and second-order joint moments of $\phi_j(t)$ are changing slowly with time is a good indication that the corresponding first- and second-order joint PDFs are slowly varying functions of time. It would seem highly unlikely that there could be a systematic cancellation of high-frequency time variations in the PDFs between different possible numerical outcomes so that the various moments are still slowly varying functions of time. Thus using the simple physical interpretable assumptions that the first and second moments of the refractive index function are slowly changing with time, we have reasoned that the first and second moments of the phase noise are also slowly changing with time, which will be used to justify assumptions made in the next sections.

### B. Filter Algorithm

After digital reconstruction has been performed [7], the result of a measurement is a stack of images showing the distribution of complex amplitude for the object wave at different times as described in Section 1. Since the light from the object is a speckle field, the intensity distribution will vary in a random manner over each image. When it comes to phase determination, image points, where the intensity happens to be low, are very sensitive to additive noise. Some of the most important sources of noise are thermal and quantization noise from the detector and additive speckle decorrelation noise due to the in-plane motion of the object speckle field in front of the objective lens caused either by in-plane motion or out-of-plane tilts of the object. When the spatial resolution is sufficiently high, a very efficient way of reducing speckle decorrelation noise is by subimage averaging as described in [8]. After averaging has been performed, the phase volume needs to be unwrapped. In the presence of the turbulent air, this is a very difficult task since small scale eddies can cause a rapid phase variation in both space and time, which leads to undersampled phase jumps and thus also

unwrapping errors. When pure temporal unwrapping is performed independently at each image point, these unwrapping errors will propagate in time away from the poorly sampled regions. To avoid this a three-dimensional (3D) branch cut unwrapping algorithm, based on the work by Huntley [9], was used. This algorithm has three majors steps. First the location of the phase singularity points are identified by calculating the total number of phase discontinuities (phase jumps that are larger than $\pi$) in closed loops around every group of four adjacent pixels in the phase volume. This number will be zero everywhere except at the location of the phase singularities. In three dimensions it can be shown that the singularity points will form closed loops in space. The second step is to create forbidden surfaces within the phase volume that prevent unwrapping paths from passing through the loops, thus making the unwrapping path independent. Finally the phase volume is unwrapped using a flood-fill type of algorithm that is described in the work by Bone [10].

One of the simplest approaches to filtering a phase volume is to treat each image point separately, and the problem thus reduces to that of filtering a single noisy time sequence. An obvious trouble with this approach is that there is no way of assuring continuity in the spatial phase distribution at a given time. A noise reduction filter capable of handling changing conditions in the noise statistics is the linear Wiener filter. An excellent review of such filters can be found in [11], but since the filter coefficients in this paper are calculated in a somewhat unconventional way, some of the material is repeated here for completeness. The filter is of the interference type, which means that it requires access to a noise sequence that is somewhat correlated with the actual noise in the sequence to be filtered. When looking at Fig. 2, it is obvious that, for nearby image points (corresponding to nearby object points), there will be a high degree of correlation between phase fluctuations because the light from these points has passed through almost the same turbulent eddies on its way to the imaging optics. By placing a rigid stationary steel grid just in front of the object to be measured, it is possible to get several reference points where the measured phase fluctuations will be due only to the turbulent air. But since the purpose of this paper is to investigate how fast the filter performance is decreasing away from one such reference point, a steel plate placed at the edge of the field of view will be used instead. There are two inputs to the filter, one sequence $x[k]$ that is measured on the stationary plate and thus only contains noise, and one sequence $d[k]$ that is measured at an arbitrary point on the moving plate. As shown in Fig. 3, $d[k]$ can be thought of as the sum a sequence $S[k]$ that is the phase variation due to the movement of the plate and $n[k]$ that is the measurement noise at this point. The sequence $d[k]$ is delayed to half the length of the filter impulse response $\bar{W}_L[k]$ so the filter can handle both positive and negative time shifts between the reference noise $x[k]$ and

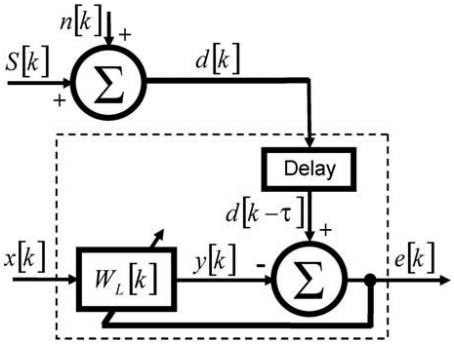

Fig. 3. Block diagram of the noise reduction filter.

the noise $n[k]$ at some specific point. Since almost nothing is known about these sequences, they must be treated as random processes. In many cases it is reasonable to assume that the movement of the plate is not affected by the turbulent air. Possible exceptions could be when the object movement is very large or when the turbulent air is created by a hot object surface. Such cases will be excluded in this paper. This means that the random process $S[k]$ will be independent from both $n[k]$ and $x[k]$. It is easy to show that the output sequence $e[k]$ will be as close as possible to $S[k]$ (for the given filter structure) in the mean squared error sense when the expectation value of $e^2[k]$ is minimized for each time $k$,

$$E\{e^2[k]\} = E\{S^2[k-\tau]\} + E\{(n[k-\tau] - y[k])^2\} + 2 \cdot E\{S[k-\tau] \cdot (n[k] - \tau - y[k])\}. \quad (6)$$

Since $S[k]$ is statistically independent from both $n[k]$ and $y[k]$, the third term will factor into products of the individual expectation values of the sequences, and if all these are assumed to be zero, the third term will vanish. It will be argued in Section 4 that this assumption can be at least approximately justified by applying a weak high-pass frequency filter to the measurement. The second term is obviously minimized when the mean-squared deviation between $n[k]$ and $y[k]$ is as small as possible, which, of course, is the same thing as saying that the mean-squared deviation between $S[k]$ and the filter output sequence $e[k]$ is as small as possible. To get a more compact notation, we introduce the data vector $\bar{X}_L[k]$ and the impulse response vector $\bar{W}_L[k]$, defined as

$$\bar{X}_L[k] = [x[k],\ x[k-1],\ \cdots,\ x[k-L]]^T, \quad (7a)$$

$$\bar{W}_L[k] = [W_0[k],\ W_1[k],\ \cdots,\ W_L[k]]. \quad (7b)$$

Now the sequence $y[k]$ can be written as the simple matrix product $y[k] = \bar{X}_L[k] \cdot \bar{W}_L[k]$. Minimizing the

expectation value of $e[k]$ is done by differentiating Eq. (3) with respect to all filter coefficients $W_0[k], \cdots, W_L[k]$ and setting the derivatives to zero, which gives a set of linear equations that can be grouped into the well-known Wiener equation for the optimum impulse response vector $\bar{W}_L^*[k]$ [6],

$$E\{\bar{X}_L[k]\cdot\bar{X}_L^T[k]\}\cdot\bar{W}_L^*[k]\triangleq R_{XX}[k]\cdot\bar{W}_L^*[k] = E\{d[k-\tau]\cdot\bar{X}_L[k]\}\triangleq P_{DX}[k]. \quad (8)$$

Now the problem is how to determine the matrix $R_{XX}[k]$ and vector $P_{DX}[k]$ that contain statistical auto- and cross correlations from a set of single realizations of the processes $d[k]$ and $x[k]$. As noted earlier the statistical mean and autocorrelation of the noise is slowly varying, and we will now make the additional assumption that the noise is "locally" ergodic around each time so its moments can be calculated from suitable local time averages using a forgetting factor [10] that reduces the contribution to the sum from samples at times far away from $k$,

$$R_{XX}[k]\approx\sum_{i=1}^{N}\lambda^{|k-i|}\cdot\bar{X}_L[i]\cdot\bar{X}_L^T[i], \quad (9a)$$

$$P_{DX}[k]\approx\sum_{i=1}^{N}\lambda^{|k-i|}\cdot d[i-\tau]\cdot\bar{X}_L[i]. \quad (9b)$$

It is, in principle, possible to solve Eq. (5) for the optimum impulse response $\bar{W}_L^*[k]$ by first calculating $R_{XX}[k]$ and $P_{DX}[k]$ from their definitions in Eqs. (9) and using Gaussian elimination, but this will be very time consuming since it has to be done at each time step. A faster way is to use recursion as done in [6], although this yields a transient behavior of the filter at the beginning because only past values of the input sequences are used to calculate the correlations. Our method uses recursion to calculate $R_{XX}[k]$ and $P_{DX}[k]$ but retains the Gaussian elimination, which means calculations will be slower but transient behavior is eliminated since all available samples are used at all times to estimate the correlations. The filter will also be noncausal (capable of handling both positive and negative time shifts between $x[k]$ and $n[k]$). $R_{XX}[k]$ and $P_{DX}[k]$ are calculated by first noting that

$$R_{XX}[k]=\sum_{i=1}^{k}\lambda^{k-i}\cdot\bar{X}_L[i]\cdot\bar{X}_L^T[i]+\sum_{i=k+1}^{N}\lambda^{i-k}\cdot\bar{X}_L[i]\cdot\bar{X}_L^T[i] = R_{XX1}[k]+R_{XX2}[k], \quad (10a)$$

$$\bar{P}_{DX}[k]=\sum_{i=1}^{k}\lambda^{k-i}\cdot d[i-\tau]\cdot\bar{X}_L[i]+\sum_{i=k+1}^{N}\lambda^{i-k}\cdot d[i-\tau]\cdot\bar{X}_L[i]=\bar{P}_{DX1}[k]+\bar{P}_{DX2}[k], \quad (10b)$$

where the terms on the right-hand side can be calculated recursively for each time step using the relations

$$R_{XX1}[k]=\lambda\cdot R_{XX1}[k-1]+\bar{X}_L[k]\cdot\bar{X}_L^T[k],$$
$$R_{XX2}[k]=\frac{1}{\lambda}\cdot R_{XX2}[k-1]-\bar{X}_L[k]\cdot\bar{X}_L^T[k], \quad (11a)$$

$$\bar{P}_{DX1}[k]=\lambda\cdot P_{DX1}[k-1]+d[k-\tau]\cdot\bar{X}_L[k],$$
$$\bar{P}_{DX2}[k]=\frac{1}{\lambda}\cdot\bar{P}_{DX2}[k-1]-d[k-\tau]\cdot\bar{X}_L[k]. \quad (11b)$$

Hence $R_{XX}$ and $P_{DX}$ only need to be calculated from their definitions at the first time step. The filtering process can be summarized in a simple three step process.

- Preparation: High-pass filter the time sequence of deformation at each image point to reduce the effect of the third term in Eq. (6) as will be discussed in Section 4.
- At the first time step: Calculate $R_{XX1}[1]$, $P_{DX1}[1]$, $R_{XX2}[1]$, and $P_{DX2}[1]$ from their definitions in Eqs. (11).
- At all later time steps:

  – Calculate $R_{XX1}[k]$, $P_{DX1}[k]$, $R_{XX2}[k]$, and $P_{DX2}[k]$ from Eqs. (11), which are then used in Eqs. (10) to determine $R_{XX}[k]$ and $P_{DX}[k]$.
  – Compute the optimum filter coefficients $\bar{W}_L^*[k]$ by Gaussian elimination in Eq. (8).
  – Compute the filter output $e[k]=d[k-\tau]-\bar{X}_L^T[k]\cdot\bar{W}_L^*[k]$. (The time delay $\tau$ is equal to half the length of the filter impulse response.)

### 3. Experimental Setup

In this paper an interferometric setup is used to measure the movement of a steel plate, ~10 cm$^2$, that is rigidly attached in one end while the other end is moved periodically back and forth using an electromagnet in connection with a signal generator. A schematic sketch of the setup is shown in Fig. 4. The peak to peak amplitude of the plate motion is ~1 $\mu$m, and it is driven with a sinusoidal frequency of ~0.1 Hz. In front of the plate, a region of air turbulence is created inside an open box (to restrict the turbulent region) using a curl tong and a soldering iron placed at right angles to the moving plate to create more temperature variation across the field of view. The soldering iron has a very precise temperature control whereas the curl tong has a high-powered heating element that is periodically turned on for ~10 s every minute. This creates a net heating of the air somewhere in the measurement. The distance from the camera to the plate is ~60 cm and the camera is an air-cooled 12 bit monochromatic PCO sensicam that has a very good dynamic range but, unfortunately, quite low sampling frequency, which complicates the phase unwrapping described in the theory part. To increase the sampling frequency (to ~22 Hz) only part of the CCD was used, giving a field of view on the plate

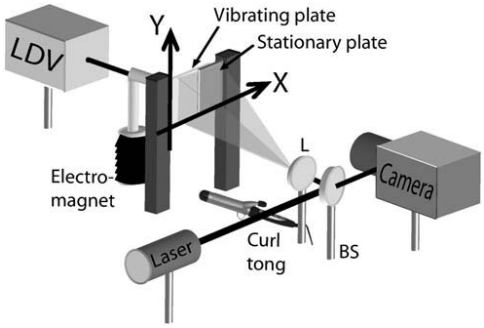


Fig. 4. Schematic of the experimental setup.

of ~8 cm horizontally and ~2.5 cm vertically. A negative lens was used to expand the reference beam, thus producing a virtual point-source in the same plane as the relay lens aperture as seen from the camera detector, which enables the use of the Fourier filtering method [5,7] for the reconstruction of the object wave-field. The laser is a continuous He–Ne laser with approximately 20 mW of output power. To be able to judge the performance of the filter, one also needs to know what the actual movement of the plate really looks like, and for that purpose the motion of the plate at one specific point is simultaneously measured using a laser Doppler vibrometer (LDV).

#### 4. Results and Discussion

Figure 5 shows an example of a measurement with the setup just described. The three lines indicate the location of the reference point ($R$) on the stationary plate where $x[k]$ used by the filter is measured and two arbitrary points ($A$ and $B$) with varying distance from $R$ where the filter performance is evaluated. When estimating the statistical correlations in Eq. (8) with suitable time averages, the filter uses a forgetting factor as discussed in connection with Eqs. (9). Choosing the optimum forgetting factor is difficult. If it is chosen too small, there will not be enough time averaging to get a good estimate, and if it is too large, you will average over regions with different statistical properties, which will also lead to a bad estimate. The best choice obviously depends on how fast the statistical properties of the noise are changing. Figure 6 shows a plot of the unfiltered deformation measured at point $A$. In the middle of the time sequence (at ~60 s), there is a rather rapid increase in the local time average of the noise because of the heating element of the curl tong being turned on. Changes in the local time average of the noise can be thought of as a change in the expectation value of the underlying random noise process. In the derivation of the optimum filter impulse response in Eq. (8), it was assumed that the expectation of both the noise and the object movement are zero at all points and for all times. If this is not the case (as in Fig. 6), the impulse response of Eq. (8) will still be the one that minimizes power in the filter output sequence, but since the third term in Eq. (6) is not zero, this does not mean the output sequence is close to actual object movement. As shown in the theory part, when the time variations of the first- and second-order moments of the refractive index are slowly varying with time, the expectation value of the phase noise will also have a slow time variation. Suppose that "slow" in this context is compared to all interesting frequencies in the object displacement. Then it is possible to apply a weak high-pass filter to the measurement, which removes the slow changes in the local time average of the noise. This will remove the time average value from the result, but this is of no consequence since object displacement is measured relative to the first image, which means that the Dirichlet boundary condition at the first image is known to be zero. If the object movement has an important slow varying component, it is still possible to reduce the effect of the third term in Eq. (6) by noting that both net heating and convection effects involve large air masses, which means the local time average in the noise will not change appreciably over the object surface (if the object is not very large). By fitting

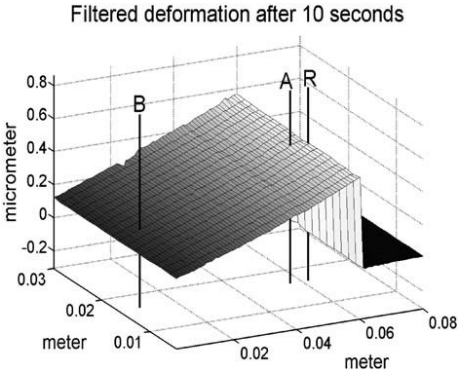


Fig. 5. Deformation of the object after 10 s.

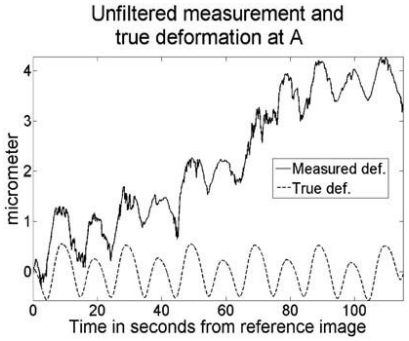


Fig. 6. Unfiltered deformation at point $A$ as a function of time (see Fig. 5) together with the true deformation.

a low degree polynomial function to the noise in $R$ and then removing this function from all points, the local time averages of both $n[k]$ and $y[k]$ will be approximately zero at all times. Figure 7 shows a plot of the mean-squared error in phase between the filtered measurement at point $A$ and the true deformation measured with the LDV as a function of the forgetting factor of the filter with and without high-pass filtering. First of all it can be noted that the deviation of the filtered sequence from the true sequence is much higher without high-pass filtering. As previously discussed this is because of the influence of the third term of Eq. (6), which has to be reduced to get good results. It can also be noted that the optimum value of the forgetting factor changes from ~0.9998 in the filtered case to ~0.992 in the unfiltered case. This is because it is possible to have a longer time averaging when the statistics (expectation value) of the noise is changing slower. Choosing a good length of the filter impulse response [$L$ in Eq. (8)] is also of great importance. Increasing the length will increase the computational time, whereas a length too short will render the filter incapable of compensating for time shifts between the noise in the point to be filtered and the reference noise. A longer impulse response will always give smaller output energy in the sequence $e[k]$, but, as shown in Fig. 8, this does not necessarily mean that the sequence is closer to the true deformation. The reason for this is that there will always be errors in the estimation of the correlations in Eqs. (9). For higher lags these correlations should usually be very small and, hence, require longer time averages to achieve the same relative accuracy as shorter lags. Experiments have shown that time shifts in the noise between different points is usually very small. When looking at Fig. 2, it is clear that a time shift between two image points due to the movement of turbulent eddies can only happen if the ray fans from the corresponding object points have a very low overlap. So the absence of time shifts could be because turbulent eddies that are small compared with the ray fans change shape or disperse much faster than they drift, leading to a decorrelation instead of a time shift. Figures 9 and 10 show the deformation after filtering at points $A$ and $B$, respectively. The impulse response length was seven samples and the forgetting factor 0.9998 (prefiltering was used). At point $A$ the signal to noise ratio was ~0.13 before filtering and ~3.3 after filtering. The corresponding signal to noise ratios at $B$ was 0.038 before filtering and 0.86 after filtering, where the decreased performance is due to decorrelation between the noise at $B$ and the reference noise at $R$. Note the two spikes at ~27 and 50 s in Fig. 9 that are due to unwrapping errors and that lower the signal to noise ratio significantly. Figure 11 illustrates in more detail how the performance of the filter varies with the distance from $R$. It shows the energy in $n[k]$, which is estimated by subtracting the LDV measurement from $S[k]$, as a function of the distance from $R$. Apparently there is some increase in the noise level away from $R$. At some points along the line away from $R$, there have been unwrapping errors (the spikes shown in Fig. 9), which have been manually removed to avoid sudden jumps in the noise energy curve. Figure 11 also shows the corresponding noise energy after filtering, which is fairly constant close to $R$ but increases rapidly at larger distances. Finally the ratio between the two noise energies is plotted since it is a good measure of how much the filter has improved the measurement at a certain point. As seen in the figure, there is actually an increase in filter performance away from $R$ at the beginning. This is because the noise is still very correlated in this region and, at the same time, the noise level is initially increasing away from $R$. Since the filter can adjust for differences in noise amplitude, it can remove more noise energy from points of initially higher noise content. However, as the distance from $R$ becomes large, the decorrelation in the noise will eventually lower the filter performance again. Figure 11 is thus also a measure of how large the correlation area is for the most important turbulent eddies. As previously mentioned there is a problem with assuring the filtered measurement will be

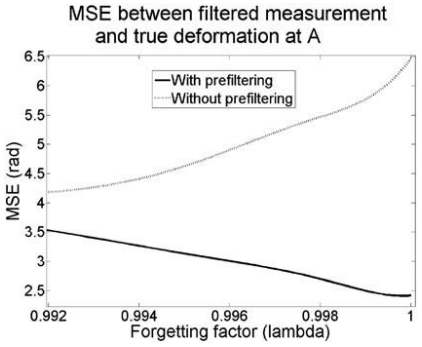


Fig. 7. MSE between the filtered measurement and true deformation as a function of the forgetting factor of the filter with and without prefiltering.

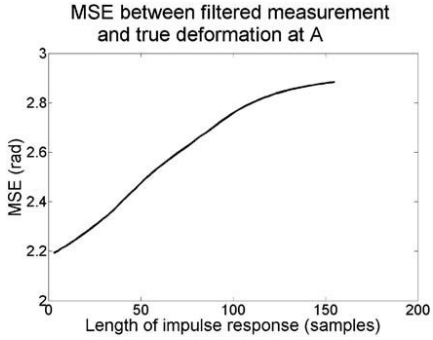


Fig. 8. MSE between the filtered measurement and true deformation as a function of the impulse response length of the filter.

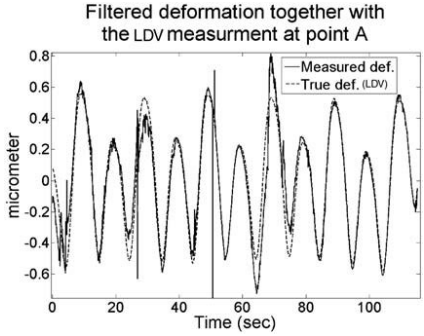


Fig. 9. Filtered deformation at $A$ as a function of time together with the true deformation.

smooth in space at each time because each point is filtered separately. However, the filter has proven very efficient at removing noise due to vibrations in the experimental setup, which tends to be highly correlated across the field of view.

## 5. Conclusions

We have considered the problem of interferometric measurements of moving and deforming objects in the presence of air turbulence and vibrations. Measurement noise has been reduced by postprocessing the data with a digital noise interference filter that uses a reference noise sequence measured on a small stationary plate that is inserted just in front of the object to reduce the noise at other image points. The method has proven successful in reducing measurement noise in a region around the reference point where there is a significant correlation in the noise. The size of this region depends on the sizes of the most important turbulent eddies in the turbulence, which, in turn, depends on the geometry and temperature of the objects causing the turbulence. Experiments have shown that sharp, hot objects such as the flame of a candle produce much smaller eddies than a coarse, cool object such as a curl tong. When looking at Fig. 2,

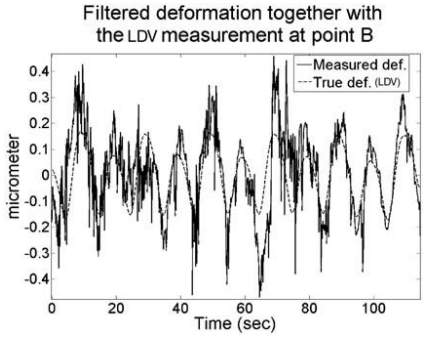


Fig. 10. Filtered deformation at $B$ as a function of time together with the true deformation.

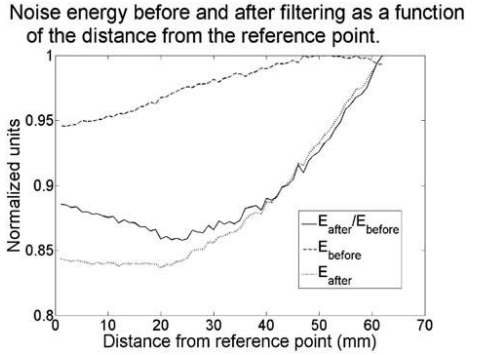


Fig. 11. Noise energy before and after filtering as a function of the distance from $R$. Energies are normalized so the maximum values are one. Also shown is the ratio of the noise energy after filtering to that before filtering (also normalized).

it is also obvious that the closer the turbulent region is to the object, the smaller the correlated region in the image will be because the ray fans are more expanded. The time sequence of object movement and deformation at each image point is filtered separately without any continuity condition between neighboring points (the filter is designed for good performance over short time intervals). Therefore at a single time instance, it is likely that the filter will introduce small discontinuities between closely spaced image points. Future work will therefore include a 3D filter implementation to avoid this problem.

## References

1. A. Labeyrie, "Attainment of diffraction limited resolution in large telescopes by Fourier analysing speckle patterns in star images," Astron. Astrophys. **6**, 85–87 (1970).
2. R. H. T. Bates and P. T. Gough, "Speckle interferometry gives holograms of multiple star systems," Astron. Astrophys. **22**, 319–320 (1973).
3. K. F. M. Tateiba, "Restoration of holographic image degraded by atmospheric turbulence and through spatial filtering," J. Electromagn. Waves Appl. **8**, 315–327 (1994).
4. L. M. H. Ullander and H. Hellsten, "Low-frequency ultra-wideband arrayantenna SAR for stationary and moving target imaging," Proc. SPIE **3704**, 35–45 (1999).
5. M. H. I. Takeda and S. Kobayashi, "Fourier-transform method of fringe-pattern analysis for computer-based topography and interferometry," J. Opt. Soc. Am. **72**, 156–160 (1982).
6. J. W. Goodman, *Statistical Optics* (Wiley, 2000).
7. P. S. S. Gren and X. Li, "Tomographic reconstruction of transient acoustic fields recorded by pulsed TV holography," Appl. Opt. **37**, 834–840 (1998).
8. J. J. M Huntley, "Random phase measurement errors in digital speckle pattern interferometry," Opt. Lasers Engineer. **26**, 131–150 1997.
9. J. J. M Huntley, "Three-dimensional noise-immune phase unwrapping algorithm," Appl. Opt. **40**, 3901–3908 (2001).
10. D. J. Bone, "Fourier fringe analysis: the two-dimensional phase unwrapping problem," Appl. Opt. **30**, 3627–3632 (1991).
11. S. T. Alexander, *Adaptive Signal Processing: Theory and Applications* (Springer-Verlag, 1986).

# Paper B

Measurement of spatio-temporal phase statistics in turbulent air flow using high-speed digital holographic interferometry.

# Measurement of spatio-temporal phase statistics in turbulent air flow using high-speed digital holographic interferometry.

**Henrik Lycksam[1*], Mikael Sjödahl[1], Per Gren[1]**

[1]Division of Experimental Mechanics, Luleå University of Technology, 971 87 Luleå,

[*]*Corresponding author: henrik.lycksam@ltu.se*

## Abstract
In this article we describe a method of measuring spatiotemporal (ST) structure and covariance functions of the phase fluctuations in a collimated light beam propagated through a region of refractive index turbulence. The measurements are performed in a small wind tunnel in which a turbulent temperature field is created using heated wires at the inlet of the test section. A collimated sheet of light is sent through the channel and the phase fluctuations across the sheet are measured. The spatial phase structure function can be estimated from a series of images captured at an arbitrary framerate by spatial phase unwrapping whereas the ST structure function requires a time resolved measurement and a full three dimensional unwrapping. The measured spatial phase structure function shows agreement with the Kolmogorov theory with a pronounced inertial subrange which is taken as a validation of the method. Due to turbulent mixing in the boundary layers close to the walls of the channel the flow will not obey Taylor's hypothesis of frozen turbulence. This can be clearly seen in the ST structure function calculated in a coordinate system that moves along with the bulk flow. At zero spatial separation this function should always be zero according to Taylor's hypothesis but due to the mixing effect there will be a growth in the structure function with increasing time difference depending on the rate of mixing.


## 1. Introduction
Imaging through turbulent media has been frequently studied in the literature. The resolution of astronomical and satellite images for example are severely degraded by the random temperature variations in the atmosphere and algorithms have been developed to improve the quality of such images. Turbulent air can also be a problem when using ground based interferometric measurement techniques such as digital holography to capture long time sequences of a moving or deforming object. In this case two additional complications arise. First of all the absolute value of the phase distortion in the object wave becomes important. Also since the object is continuously moving and/or deforming it is not possible to capture a long sequence of images and use "ensemble averaging" techniques such as speckle imaging [1], [2]. One way of reducing the effects of phase noise in such a measurement would be to use a digital spatiotemporal (ST) noise reduction filter but this requires knowledge of the ST statistics of the phase fluctuations. Yamauchi and Hibino have studied the temporal statistics of the phase fluctuations in interferometric measurements performed on a small lens mold during processing in a grinding machine [3]. When measuring on larger objects the spatial variations in the noise cannot be ignored [4] and full ST statistics is required. This article describes a method for measuring ST phase structure and covariance functions for the case of temperature fluctuations that have at least stationary time increments using high-speed digital holographic interferometry. Non stationary fluctuations, such as those generated during heat molding, are difficult to deal with

and will be excluded. The method is applied to the relatively simple case of quasi homogenous/isotropic turbulence generated in a wind tunnel for which the Kolmogorov theory applies. Thus it is possible to verify the method against the theory. The article is organized as follows. Section 2 describes both the measurement setup and the wind tunnel for creating the refractive index fluctuations. Section 3 contains a short summary of theoretical expressions for phase structure functions in locally inhomogenous/isotropic medium. Section 4 describes how the phase structure and covariance functions are estimated from the measured phase volume. Section 5 shows some of the measurement results and a comparison with the theory of section 3. Section 6 discusses what conclusions can be drawn from this work.

## 2. Experimental setup

There are many ways to generate a turbulent temperature variation in a flow of air. A common approach is to force the air through a grid which tends to give turbulence with good homogeneity and isotropy properties. The problem with grid turbulence is that it is difficult to produce turbulence with an inertial subrange in their energy spectra. This is because the Reynolds number associated with the grid needs to be very high, which according to the work of Corrsin [5] is difficult to achieve in a conventional smaller sized wind tunnel. A way around this problem is to use an active grid which has been done by many authors [6]. Another way of achieving a turbulent flow is to stir an otherwise laminar flow in a random manner using different kinds of moving “wings” upstream of the test section as done by Makita [7]. Turbulence can also be produced in the bulk air flow inside a wind tunnel provided the Reynolds number is high enough. This is not an ideal solution because a very long test section is required for the turbulence to get reasonably homogenous and this also means that large turbulent boundary layers will form. But as noted by Strohbehn [8] the temperature fluctuations tend to homogenize at a faster rate than the velocity fluctuations and therefore this approach is not as bad as it might seem. Indeed, Magee and Welsh [9] have succeeded in constructing a small desktop flow channel with a very short test section that produced relatively homogenous refractive index disturbances with an inertial subrange covering about an order of magnitude in spatial frequencies. In this article we have used a wind tunnel with a test section of about one meter to generate boundary layers that are large enough to cause significant violation of the frozen turbulence hypothesis and thus nontrivial ST statistics.

Figure 1 shows a sketch of the experimental setup. The light source is a continuous Nd:YAG laser with an output power of about 0.4 W. Light from the laser is split into a reference- and object beam using a half wave plate ($\lambda/2$) and a thin film polarizer (P) so that the relative intensity of the two beams can be adjusted. The object beam is expanded into a thin sheet using two cylindrical lenses and collimated using the positive lens (L1). The collimated light sheet is sent through slits in the channel to a diffuser plate on the other side of the channel which is imaged onto the detector of a high speed camera (redlake MotionPro X). It is important to make sure that the spatial resolution on the diffuser plate is so high that the smallest temperature inhomogenities (that makes a significant contribution to the phase fluctuations) are resolved. Otherwise there will be errors in the estimation of the structure and covariance functions due to spatial averaging in the measurement. The maximum width of the sheet is therefore limited to a few centimeters. The reference light is sent through a fiber (F) and expanded using a negative lens (L3). Reconstruction of the holograms is done using the Fourier filtering method [10, 11].

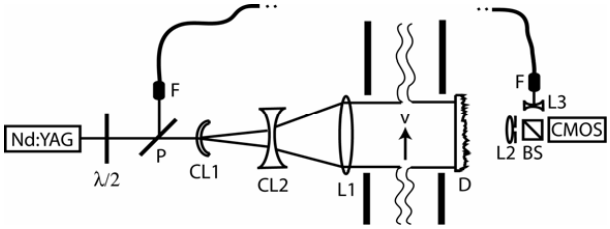


Figure 1: Sketch of the experimental setup. λ/2 is a halfwave plate and P is a thin film polarizer. CL1 and CL2 are cylindrical lenses and L1,L2,L3 are ordinary single lenses. D is a diffuser plate and BS a beamsplitter cube. CMOS is the high-speed camera.

The wind tunnel (see figure 2) is homebuilt and composed of the following parts. First is a settling chamber (S) made of straws and a metallic grid that breaks down large turbulent eddies in the outside air. Next is a contraction cone (C) where the cross section of the flow is gradually decreased to that of the test section (10x40 cm). At the start of the test section is a small strip of sandpaper to aid the transition to a turbulent flow. This will also speed up the transition from laminar to turbulent boundary layer growth. Next to the sandpaper are five heated canthal wires (HW) to provide an initial large scale temperature variation that is successively broken down by the velocity fluctuations. After the test section is a diffuser (DI) to lower the air velocity at the fan. The object light sheet is sent through a pair of rotatable slits (RS) that are positioned 90 cm from the inlet of the test section. In our experiments the light sheet was aligned with the direction of the flow. The flow is driven by a commercial 135 W ventilation fan (F) with a speed range of 450 to 1260 rpm corresponding to a velocity range of 2.7-8.2 m/s in the test section. The optical components are mounted on an air damped optical table with the channel running 10 cm above it without being in direct contact to avoid excessive transfer of vibrations.

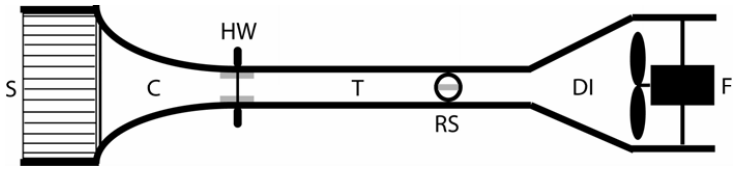


Figure 2: Sketch of the wind tunnel used to produce the turbulent air. S is the settling chamber and C the contraction cone. HW are the heated chantal wires inside the test section T. RS are the rotatable slits, DI the diffuser and F the fan.

## 3. Theory

Light propagation in locally homogenous/isotropic media has been extensively studied in the literature [12], [13],[14]. The following is meant as a short summary of the theoretical results that are important in this article. Figure 3 shows the geometry of the light propagation problem.

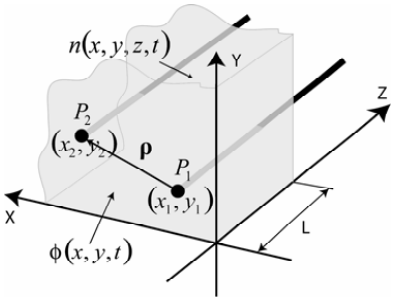


Figure 3: Light propagation geometry. The refractive index fluctuations in the turbulent region of size $L$ are $n(x,y,z,t)$. $\phi(x,y,t)$ is the phase fluctuations of the wave in the detector plane. $\boldsymbol{\rho}$ is the vector between two points $P_1$ and $P_2$ in the detection plane with coordinates $(x_1,y_1)$, $(x_2,y_2)$.

An initially plane wave enters a region of refractive index fluctuations described by $n(x,y,z,t)$ and propagates a distance $L$ through the disturbed region. The phase distribution $\phi(x,y,t)$ finally appears in the xy-plane. It is fortunate that the structure function of $\phi(x,y,t)$ is the same regardless of the length of propagation [15]. This means that is it possible to imagine the light rays as being perfectly straight as in figure 3. In noninterferometric imaging through turbulent media there is a distinct advantage of using structure functions instead of correlation functions to describe the phase fluctuations because the turbulent structures that are large compared to the pupil of the imaging system doesn't cause any significant image degradation. These large structures are the ones that are most dependent on the geometry of the turbulent flow and hence by cancelling out there effect the fluctuations will be more homogenous and isotropic. Therefore most of the theoretical work on phase fluctuations being published has concentrated on these structure functions. It will be assumed that the mean of $\phi(x,y,t)$ changes slowly with time compared with the random fluctuations ($\phi(x,y,t)$ is said to have stationary time increments) and also compared to all time differences used in the ST structure function. Even though the strength of the turbulence can change over time it is customary, at least in the atmospheric literature, to exclude the time dependence of the phase structure function. In this case the spatial structure function ${}^{S}D_{\phi}$ can be expressed as [12]:

$$ {}^{S}D_{\phi}(x_1,y_1,x_2,y_2) = \left\langle \left[\phi(x_1,y_1,t) - \phi(x_2,y_2,t)\right]^2 \right\rangle \tag{1} $$

where $\langle\ \rangle$ is the expectation value operator. In the case of a locally homogenous/isotropic flow with constant fluctuation strength ${}^{S}D_{\phi}$ will only depend on $\rho$, the distance between points $P_1$ and $P_2$, and have a simple functional form independent of the flow geometry [12]:

$$ \begin{aligned} {}^{S}D_{\phi}(\rho) &= 2.91 \cdot k^2 \cdot C_n^2 \cdot L \cdot \rho^{5/3} \qquad l_0 << \rho << L_0 \\ {}^{S}D_{\phi}(\rho) &= 3.44 \cdot k^2 \cdot C_n^2 \cdot L \cdot l_0^{-1/3} \cdot \rho^2 \qquad \rho << l_0 \end{aligned} \quad . \tag{2} $$

Here $k$ is the vacuum wavenumber of the light and $l_0$ the inner scale of the refractive index fluctuations (roughly speaking the size of the smallest inhomogenities). The structure constant $C_n^2$ is a measure of the strength of the refractive index fluctuations. In cases where the fluctuation strength varies slowly with time it is customary to include this time dependence in

$C_n^2$ [13]. Here it is assumed that $C_n^2$ is constant along the whole propagation path. If this is not true $C_n^2$ must be replaced by an integral over the propagation path [15]. In our experiments it is the first equation in (2) that will be used to validate the method. In the same way as in equation (1) the ST phase structure function ${}^{ST}D_\phi$ can be expressed as:

$$ {}^{ST}D_\phi(x_1, y_1, x_2, y_2, \tau) = \left\langle [\phi(x_1, y_1, t) - \phi(x_2, y_2, t+\tau)]^2 \right\rangle \tag{3}$$

Assuming for the moment that Taylor's hypothesis of frozen turbulence holds perfectly, the refractive index inhomogenities will simply move across the region of detection in the xy-plane at the bulk flow velocity $\mathbf{V_0}$ without evolving or mixing. The effect of the $V_{0z}$ velocity component parallel to the light propagation direction in figure 3 is simply to decrease the correlation between the phase fluctuations at $P_1$ and $P_2$ because during time $\tau$ some turbulent eddies will have drifted out of the propagation path being replaced by others. As argued by Tatarskii [13] this decorrelation effect is usually not important because for long propagation lengths it takes a very long time difference before the effect becomes noticeable and by that time movement perpendicular to the flow will in general be so large that the fluctuations at the two points will be fully decorrelated anyway. However when doing experiments where the observation area is large and propagation lengths rather small (for example to study turbulent mixing in a free flow) this effect can become important. Ignoring the effect of the flow parallel to the light propagation direction the ST phase structure function is:

$$ {}^{ST}D_\phi(\boldsymbol{\rho}, \tau) = {}^{S}D_\phi(|\boldsymbol{\rho} - \mathbf{V_{0\perp}} \cdot \tau|) \tag{4}$$

where $\mathbf{V_{0\perp}}$ is component of the bulk flow velocity in the xy-plane (detectorplane) in figure 3. Taylor's hypothesis can of course never be strictly valid because there will always be small random velocity fluctuation in the flow (otherwise there would be no random temperature variations to begin with). When there are mixing of the turbulent eddies the ST structure function ${}^{ST}D_\phi(\mathbf{V_{0\perp}} \cdot \tau, \tau)$ will not be zero for all $\tau$ as suggested by equation (4). Physically ${}^{ST}D_\phi(\mathbf{V_{0\perp}} \cdot \tau, \tau)$ can be interpreted as the structure function with zero spatial separation calculated in a coordinate system that moves along with the flow. In the case of a channel flow there are two sources of mixing, the deterministic mixing due to a nonuniform bulk velocity and the random velocity fluctuations. Once the ST structure function has been measured it is easy to determine the velocity component $\mathbf{V_{0\perp}}$ by finding the separation $\boldsymbol{\rho}_{\mathbf{min}}$ that minimize $D_\phi(\boldsymbol{\rho}, \tau)$ for a given $\tau$ :

$$ \mathbf{V_{0\perp}} = \frac{\boldsymbol{\rho}_{\mathbf{min}}}{\tau} . \tag{5}$$

In noninterferometric imaging the phase structure function is sufficient information to determine the image degradation (long and short exposure OTF of the atmosphere). But in an interferometric measurement the lower spatial frequencies of the refractive index turbulence are just as important as the higher frequencies and hence it would be desirable to determine the phase covariance function instead. Unfortunately these coarse refractive index variations are highly dependent on the flow geometry and therefore usually not homogenous and isotropic which means that the covariance function will depend on absolute coordinates. Since there is no

simple theory for the coarse refractive index variation the covariance function will be expressed only in terms of the measured phase distribution $\phi(x,y,t)$. To enable the estimation of the covariance function from a single measured phase volume it must be assumed that $\phi(x,y,t)$ is wide sense stationary in time with zero mean,

$$C_\phi(x_1,y_1,x_2,y_2,\tau)=\langle\phi(x_1,y_1,t)\cdot\phi(x_2,y_2,t+\tau)\rangle\,. \tag{6}$$

It should be mentioned that Vecherin et al. [16-18] have successfully used homogeneous and isotropic Gaussian ST covariance functions to approximately describe the full three dimensional temperature field of a limited region of the atmosphere for recording tomographic images of temperature inhomogenities.

## 4. Estimation of statistics from the measured phase volume

The procedure for estimating the spatial structure function, spatiotemporal structure function and covariance function for the phase fluctuations is illustrated in figure 3.

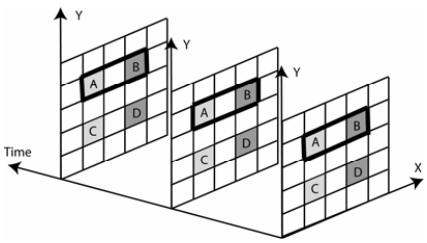


Fig 3: Shows part of a measured phase volume where A, B, C, D are phase elements at different points in the image.

When estimating the spatial phase structure function the camera can be run at a relatively low frame rate so that the phase noise in the different images are fairly independent. This will reduce the amount of data necessary to get a good estimate. The random phase contribution from the diffuser plate is compensated for by capturing a reference image before the wind tunnel is switched on and then multiplying all of the measured complex amplitude distributions with the complex conjugate of this reference image. Figure 3 shows a sketch of part of a measured phase volume. The spatial phase structure function was first estimated using equation (1) i.e. it was not initially assumed that the flow was locally homogenous/isotropic. For a pair of points (A,B) this means that only temporal averaging was performed. Since it is only the phase difference between the two points that is important it is possible to use a two-dimensional spatial unwrapping of each image separately. In our experiment we used only a sheet of light and hence the phase volume had only one spatial dimension and a simple one-dimensional unwrapping between the points was sufficient as illustrated by the solid box around the AB point pair. If, as in our measurement, the fluctuations turn out to be locally homogenous/isotropic then all pair of point with the same separation e.g. AB, CD, AC, BD can be used in the averaging.
The ST structure and covariance functions need to be estimated from a measurement in which the phase fluctuations are resolved in time. Here another procedure was chosen to remove the random phase contribution from the diffuser plate. The time sequence at each measurement point is unwrapped independently and then adjusted against each other by removing the average value of each sequence. This is possible because the measurement time is much longer than the longest characteristic phase fluctuation time. This method was chosen because it both removes the

effects the diffuser plate and the need to perform a difficult and time consuming three-dimensional unwrapping. When studying self-convective flows where the fluctuation times can be very long it is necessary to use the previous method for removing the effects of the diffuser plate together with a real three-dimensional unwrapping procedure. The procedure for estimating the ST structure function is then completely analog to the spatial case except that one of the phase elements in figure 3 is taken from a later image. As mentioned in connection with equation (6) the covariance cannot always be estimated from a single phase volume such as that in figure 3. Because the measured phase $\phi(x,y,t)$ is usually not homogenous/isotropic it needs to be wide sense stationary in time, otherwise no averaging at all is possible in the phase volume. This is a reasonable assumption for a stationary channel flow such as that used in our experiment but it doesn't hold for the very important class of self convective flows. However we have previously, with some success, used a method of local time averaging [19] to estimate the temporal correlation of the phase fluctuations in such a flow and this method can easily be extended to the ST case. Choosing an appropriate frame rate can be done by looking at the temporal spectra of the phase fluctuations. Assuming that Taylor's hypothesis holds the temporal spectral density $W_\phi$ depends only on the one dimensional spatial spectral density $V_\phi$ of the phase and the magnitude of the bulk flow velocity $v_{0\perp} = |\mathbf{V}_{\mathbf{0}\perp}|$ perpendicular to the light propagation according to [13]:

$$W_\phi(f) = \frac{1}{v_{0\perp}} \cdot V_\phi\left(\frac{f}{v_{0\perp}}\right) \tag{7}$$

where $f$ is the temporal frequency. The effects of turbulent mixing of eddies will manifest itself mostly for low time-frequencies which means that it plays no role in estimating the bandwidth. The highest spatial frequency will approximately be that corresponding to the inner scale size ($\sim 1/l_0$) which can be estimated from the spatial structure function. Hence from equation (7) the highest time frequency will be:

$$f_{\max} \approx \frac{v_{0\perp}}{l_0}. \tag{8}$$

Since most of the energy in the spatial fluctuations are concentrated to lower frequencies it may not be necessary to choose the sampling frequency as high as $2f_{\max}$ in an actual experiment. In our experiments the sampling frequency was chosen to be just over $f_{\max}$.

## 4. Results and discussion

Figures 4 and 5 show the estimated spatial phase structure functions for flow velocities of 8.2 and 2.7 m/s, respectively, in the test section. This corresponds to Reynolds numbers of about 53000 in figure 4 and 18000 in figure 5 which means that the turbulence should be fully developed. The structure function was first estimated using equation (1) to check that the flow really was locally homogenous/isotropic across the 15mm wide light sheet which is aligned with the flow. The spatial resolution is about 0.07 mm which, according to the work of Magee and Welsh [9], should be well below the inner scale size. They used a channel of similar geometry and flow speeds and there measurements showed inner scale sizes of about 0.4-1 mm. Also plotted are curves fitted from equations (2). The inner scale size $l_0$ is chosen as the separation for which the measured curve starts to deviate from the curve fitted from the first equation in (2). The values of the structure constant $C_n^2$ are about $10-10^6$ times stronger than typical near ground atmospheric

conditions [8]. For small separation the measured curves tend to curve upwards instead of downwards as suggested by the theory. We believe that this is due to the large boundary layers close to the wall of the channel which contains more fine structures than the bulk flow. The sampling rate was 100 Hz which means that the air will have moved about 46 mm between each image so that the phase fluctuations will be fairly independent. The total number of images was 15000.

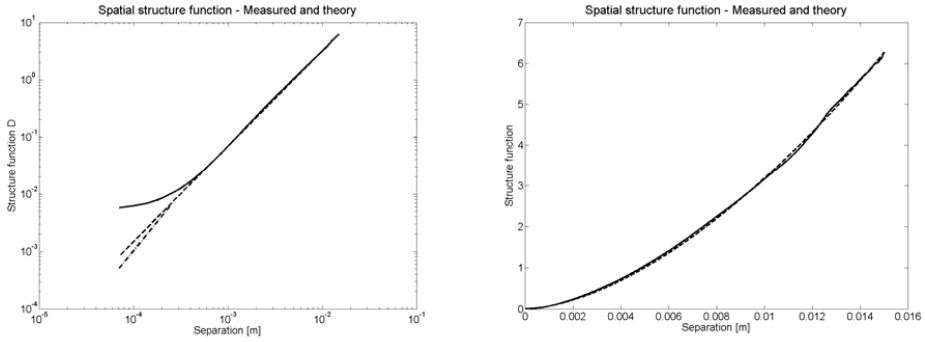


Figure 4: Spatial phase structure function with a flow velocity of 8.2 m/s and a Reynolds number of about 53000. Also shown are theoretical curves fitted from equation (2) with $C_n^2 = 3.8 \cdot 10^{-11} m^{-2/3}, l_0 \approx 0.5mm$.

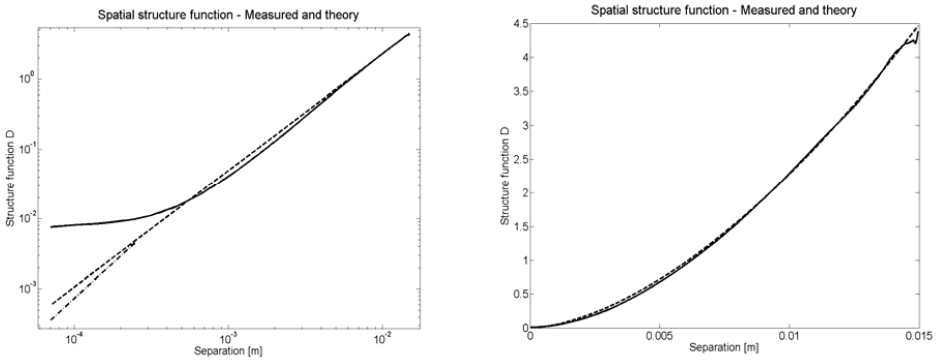


Figure 5: Spatial phase structure function with a flow velocity of 2.7 m/s and a Reynolds number of 18000. Also shown are theoretical curves fitted from equation (2) with $C_n^2 = 3.4 \cdot 10^{-11} m^{-2/3}, l_0 \approx 0.5mm$.

Figure 6a shows an estimated spatiotemporal phase structure function for three different time delays. The flow velocity in the test section was 4.6 m/s. This velocity was measured using a sensitive pitot tube but it can also be very accurately estimated from equation (5).
The structure function was first estimated using equation (3) to verify that the flow really is locally homogenous/isotropic across the 56 mm wide light sheet which is align with the flow. In this case the spatial resolution is about 0.26 mm which might not be adequate to really resolve the smallest structures but from figures 4 and 5 we know that there is a good agreement with the Kolmogorov theory so that result need not be repeated here. The sampling rate was 10 kHz

which is to be compared with the highest temporal frequencies estimated to 9 kHz using equation (8) with $l_0 \approx 0.5\,\text{mm}$ and $v_{0\perp} = 4.6\,\text{m/s}$. As mentioned in connection with equation (8) this apparent undersampling is probably not important because most of the fluctuation energy is contained in the larger spatial structures (lower temporal frequencies). Because of the high sampling rate necessary to resolve the fluctuations in time combined with the need to average over many independent fluctuations the necessary amount of images to get a reasonable estimate becomes very high. In this case the total number of images was 104791 (limited by the camera memory). Figure 6b shows the phase covariance function estimated from the same measurement. It was first estimated using equation (6) but as it turned out the flow was very homogenous along the 56 mm light sheet and so the covariance function is simply a function of the magnitude of the separation along this sheet. Had the slit been rotated 90 degrees there would have been larger variations in the statistics, but because the fluctuations are wide sense stationary in time it would still have been possible to use equation (6) to estimate the covariance function. As mentioned in the introduction the main purpose of estimating the ST statistics of the phase fluctuations is to use them in combination with a ST noise reduction filter to post process measurements of object deformation/movement performed in a disturbed environment. When calculating, for example, the ST phase covariance function from such a measurement the result will be the sum of the ST covariance function of the object and the air. If the object motion doesn't exactly match the bulk flow velocity of the air the covariance functions of the air and object will, for sufficiently large time differences, be separated. When looking at figure 6b it is obvious that the shape of the covariance function of the air for small time differences could be estimated from the corresponding covariance function for a larger time difference. Hence the bulk flow of the air (which exist even in self-convective flows) can be used to separate the covariance functions of the object and air. The reason that the covariance function is homogenous and thus very similar to the structure function is probably that the nature of the turbulent flow changes very little in the downstream direction across the relatively narrow light sheet.

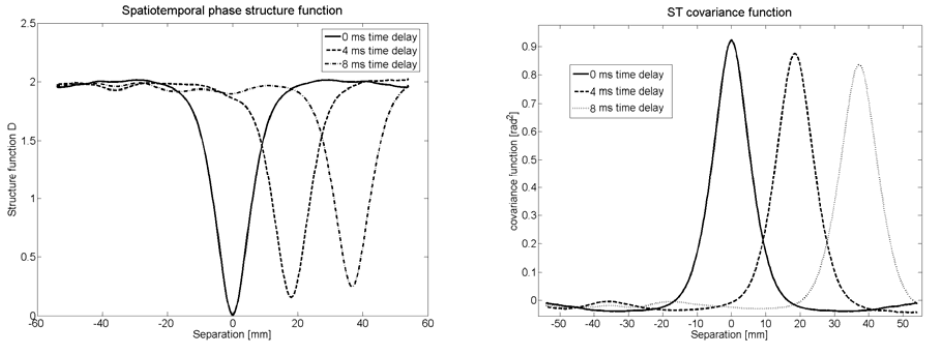


(a) (b)

Figure 6: ST phase structure and covariance function for a flow velocity of 4.6 m/s.

Figure 7 shows a plot of ${}^{ST}D_{\phi}\left(\mathbf{V}_{\mathbf{0}\perp}\cdot\tau,\tau\right)$ as a function of time difference for a flow speed of 2.7 m/s in the test section. The largest allowable time difference is limited by the flow velocity and the size of the observation region. The rapid growth at the end is because ${}^{ST}D_{\phi}\left(\mathbf{V}_{\mathbf{0}\perp}\cdot\tau,\tau\right)$ is calculated simply as the min value of the ST structure function in figure 6a and when the min value drifts out of the observation region this value will be rapidly growing until it reaches its maximum value. For small time delays most of the growth in ${}^{ST}D_{\phi}\left(\mathbf{V}_{\mathbf{0}\perp}\cdot\tau,\tau\right)$ is likely to be due

to the rapid mixing of eddies inside the boundary layers. The exact shape of ${}^{ST}D_{\phi}(\mathbf{V}_{\mathbf{0}\perp}\cdot\tau,\tau)$ as a function of $\tau$ will depend on the size distribution of eddies in the boundary layer, the variation in fluctuation strength across the boundary layer and the velocity profile. For large time delays the contribution from the boundary layers to ${}^{ST}D_{\phi}(\mathbf{V}_{\mathbf{0}\perp}\cdot\tau,\tau)$ will eventually settle towards a constant value (equal to twice the phase variance over the layer). The effect of the turbulent mixing inside the bulk flow will then be the dominant contribution to the growth of ${}^{ST}D_{\phi}(\mathbf{V}_{\mathbf{0}\perp}\cdot\tau,\tau)$. In this region the growth will depend on the magnitude of the random velocity fluctuation compared to the mean flow velocity. Using an array of cameras it would be possible in principle to follow the flow for a long enough time to be able to see how ${}^{ST}D_{\phi}(\mathbf{V}_{\mathbf{0}\perp}\cdot\tau,\tau)$ behaves in this region. But because the range of time delays are very limited in figure 7 it is difficult to draw any quantitative conclusions from it. It would be interesting to investigate whether it is possible to determine the change in shape of the whole ST structure function from curve in figure 7 alone.

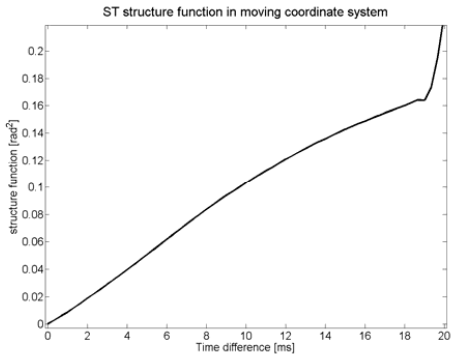


Figure 7: ST phase structure function at zero separation in a coordinate system moving along with the flow.

## 5. Conclusions

Interferometric measurement techniques such as digital holographic interferometry require that the phase disturbances due to temperature inhomogenities in the surrounding air do not change during the time of the measurement. This is a problem when performing a time resolved measurement of the movement and/or deformation of an object over a time that is longer than the fluctuation time of the inhomogenities. Since the object is continually changing it is not possible to use classical image enhancement techniques such as speckle imaging [1], [2] to reduce noise in the measurement. Using a digital noise reduction filter is possible but requires that the some statistics of the phase fluctuations are known. In this article we have developed a method for estimating spatiotemporal phase structure and covariance functions in a turbulent air flow using high-speed digital holographic interferometry.

The method has been applied to the case of locally homogenous/isotropic refractive index turbulence generated in a small wind tunnel. The measured structure functions show good agreement with the Kolmogorov theory which is taken as a validation of the method. It is also shown that the spatiotemporal structure function contains information about the bulk flow velocity and the turbulent mixing of eddies inside the flow. For the case of measuring an object deformation/movement in the presence of refractive index fluctuations a method of separating the ST statistics of the object and air is also suggested.

## 6. References


1. A. Labeyrie, "Attainment of Diffraction Limited Resolution in Large Telescopes by Fourier Analyzing Speckle Patterns in Star Images," Astron. & Astrophys. **85**(1970).
2. K. T. Knox and B. J. Thompson, "Recovery of images from astronomically degraded short exposure images," Astrophys. J. **193**(1974).
3. M. Yamauchi and K. Hibino, "Measurement of air turbulence for on-machine interferometry," Applied Optics **42**(2003).
4. H. Lycksam, "Wiener filtering of interferometry measurements through turbulent air using an exponential forgetting factor," Applied Optics **47**, 2971-2978 (2008).
5. S. Corrsin, "Local isotropy in turbulent shear flow," NACA-RM-58B11 (1958).
6. S. Ozono, "Turbulence generated in active-grid mode using a multi-fan wind tunnel," Journal of Wind Engineering and Industrial Aerodynamics **94**, 225-240 (2006).
7. H. Makita, "Realization of a large-scale turbulence field in a small wind tunnel," Fluid Dynamics Research **8**, 53-64 (1991).
8. J. W. Strohbehn, ed., *Laser beam propagation in the atmosphere* (Berlin, 1978).
9. E. P. Magee and B. M. Welsh, "Characterization of laboratory generated turbulence by optical phase measurements," SPIE **2005**(1993).
10. M. Takeda, H. Ina, and S. Kobayashi, "Fourier-transform method of fringe-pattern analysis for computer-based topography and interferometry," Journal of the Optical Society of America **72**, 156-160 (1982).
11. P. Gren, S. Schedin, and X. Li, "Tomographic reconstruction of transient acoustic fileds recorded by pulsed TV holography," Applied Optics **37**(1998).
12. V. I. Tatarskii, *Wave Propagation in a Turbulent Medium* (Dover Publications, Inc. , New York, 1961).
13. V. I. Tatarskii, *The effects of the turbulent atmosphere on wave propagation* (Israel Program for Scientific Translations, Jerusalem, 1971).
14. L. A. Chernov, *Wave Propagation in a Random Medium* (McGraw-Hill, New York, 1960).
15. J. W. Goodman, *Statistical Optics* (John Wiley & Sons, Inc., New York, 1985).
16. S. N. Vecherin, V. E. Ostashev, G. H. Goedecke, D. K. Wilson, and A. G. Voronovich, "Time-dependent stochastic inversion in acoustic travel-time tomography of the atmosphere," J. Acoust. Soc. Am. **119**, 2579-2588 (2006).
17. S. N. Vecherin, V. E. Ostashev, A. Ziemann, D. K. Wilson, K. Arnold, and M. Barth, "Tomographic reconstruction of atmospheric turbulence with the use of time-dependent stochastic inversion," J. Acoust. Soc. Am. **122**, 1416-1425 (2007).
18. S. N. Vecherin, V. E. Ostashev, and D. K. Wilson, "Three-Dimensional Acoustic Travel-Time Tomography of the Atmosphere," Acta Acustica **94**, 349-358 (2008).
19. H. Lycksam, M. Sjödahl, P. Gren, and J. Leblanc, "Wiener filtering of interferometry measurements through turbulent air using and exponential forgetting factor," Applied Optics **47**(2008).